Synaptic vesicles that store monoamines and glutamate differ in protein composition.

Hrach Asmerian[1*], Alexia J. Diaz[1*], Hongfei Xu[2], Juan A. Oses-Prieto[3], Jacob Alberts[1], Anna Sanetra[1], Barathan Gnanabharathi[1], Noah Carr[1], Alma L. Burlingame[3], Robert H. Edwards[2], Kätlin Silm[1#]

Author affiliations:

[1]Center for Neural Science and Medicine, Board of Governors Regenerative Medicine Institute, Departments of Biomedical Sciences and Neurology, Cedars-Sinai Medical Center, Los Angeles, CA, USA.

[2]Departments of Physiology and Neurology, University of California, San Francisco School of Medicine, San Francisco, CA, USA.

[3]Department of Pharmaceutical Chemistry, University of California, San Francisco School of Medicine, San Francisco, CA, USA.

[#]Corresponding author: Katlin Silm, Katlin.silm@cshs.org

*Equal contribution

ABSTRACT

Neuromodulators such as the monoamines are known to differ from classical neurotransmitters like glutamate in the time scale of signaling due to activation of slower G protein-coupled receptors. Recent work has suggested that the mode of release also differs between classical and modulatory transmitters. Although many components of neurotransmitter release machinery have been identified, we still understand little about the mechanisms responsible for differences in release. In this study, we address the differences between release of dopamine and glutamate by comparing the composition of synaptic vesicles (SVs) that contain the vesicular monoamine transporter 2 (VMAT2) versus vesicular glutamate transporter 2 (VGLUT2). Previous work has shown that these SV populations differ in frequency dependence, recycling kinetics and biogenesis. Taking advantage of a CRISPR-generated knock-in mouse with a cytoplasmic hemagglutinin (HA) tag at the N-terminus of VMAT2 to immunoisolate monoamine SVs, we find differences in the abundance and isoform expression of many SV protein families. Validation in primary neurons and in brain tissue confirms these differences in SV protein abundance between dopamine and glutamate release sites. Functional analysis reveals that the loss of differentially

expressed SCAMP5 selectively impairs the recycling of VGLUT2 SVs, sparing VMAT2 vesicles in the same neuronal population. These findings provide new insights into the molecular diversity of SVs and the mechanisms that regulate the release of dopamine and glutamate, with implications for the physiological role of these transmitters and behavior.

INTRODUCTION

Considerable work over decades has elucidated the basic machinery of neurotransmitter release[1–3] but many questions remain about the molecular mechanisms that account for the diversity in release properties at different synapses. Differences in release have been observed between neuronal populations, but also individual release sites made by the same axon, and even between vesicles in the same terminal[4–12]. This points to contribution from cell-wide differences in the expression of synaptic proteins[13–16] but also to local mechanisms at synaptic sites, which can be further modulated by postsynaptic neurons[4,6,8,10,17]. Furthermore, most of our understanding of neurotransmitter release derives from work conducted in neurons that use fast, synaptic signaling. In contrast to classical transmitters like glutamate and GABA which activate ionotropic receptors, neuromodulators such as monoamines are often released at sites without a direct postsynaptic target[18] and activate G-protein coupled receptors which signal over longer times scales[19]. Despite critical roles in normal brain function, the molecular regulation of the release of dopamine and other modulatory monoamine transmitters remains poorly understood.

While dopamine neurons fire tonically at low frequencies, dopamine release is significantly increased during high frequency burst firing, and this is central to reinforcement learning[20]. This property of dopamine release requires the recruitment of synaptic vesicles (SVs) specifically at high frequency. Indeed, it has been shown that dopamine release is more loosely coupled to Ca^{++} entry than fast synaptic release[21,22], consistent with a lower probability of release in response to isolated stimuli, and a large increase with the accumulation of presynaptic Ca^{++} at high frequency. Recent evidence also suggests that dopamine is only released from a subset of axonal varicosities[23], which could reflect the sparsity of active zones in dopamine axons[24–26]. These findings suggest that the machinery for release in dopamine neurons differs from the standard model at classical synaptic sites.

Beyond the cell type specific features of dopamine axons, recent work in neurons that release both dopamine and glutamate has shown that the two transmitters differ in release even from the

same neuron[22]. This is mediated by their storage in functionally distinct SVs that differ in synaptic recycling kinetics and in frequency dependence of fusion, which leads to faster depression of glutamate release[22]. Indeed, the formation of SVs that store monoamines relies heavily on a pathway that involves the adaptor protein complex 3 (AP-3)[22,27]. While previous work that addressed the role of this adaptor in other neuronal populations found a minor effect on the SV cycle[28,29], loss of AP-3 leads to a severe reduction in the synaptic recycling of pHluorin-tagged vesicular monoamine transporter 2 (VMAT2)[22,27]. This defect in turn reduces dopamine release in the dorsal striatum and is especially pronounced at high stimulation frequencies[27]. Indeed, these results are compatible with observations from multiple studies demonstrating that AP-3-dependent SVs preferentially fuse during high frequency activity[27,30,31]. Strikingly, the recycling of the vesicular glutamate transporter 2 (VGLUT2) that mediates glutamate corelease in dopamine neurons is not affected by the loss of AP-3[22,27,30,32–34]. This suggests that VGLUT2 is excluded from AP3-dependent SVs and targets to a subpopulation of vesicles that likely form via the classical AP2-dependent mechanism[29,35]. AP-3-independent vesicles also contribute to tonic dopamine release during low levels of activity as demonstrated by the more modest effect of the AP-3 knock-out on dopamine release with stimulation at low frequency[27]. Differential reliance of VMAT2 and VGLUT2 on the AP-3 pathway was also shown to extend beyond neurons that release multiple transmitters[12,27,30]. Compatibly with this model, VGLUT2-dependent glutamate release is consistently found to have high initial probability and to undergo depression with sustained activity[5,7,30,36,37]. The differential reliance on AP-3 suggests that differences in the biogenesis of VMAT2$^+$ versus VGLUT2$^+$ SVs contribute to the differences in release, likely by affecting SV composition.

Compositional diversity among SVs has previously been addressed by comparing vesicles that store the principal fast excitatory and inhibitory transmitters glutamate and GABA[38]. This comparison identified few differentially expressed proteins, suggesting a relatively uniform composition of SVs across neuronal populations. In the present study, we focus on SV populations that contain VMAT2 or VGLUT2 but also differ in biogenesis mechanism and release properties.

RESULTS

Proteome of VMAT2$^+$ and VGLUT2$^+$ synaptic vesicles. Due to the limited reliability of VMAT2 antibodies, we used CRISPR to generate a knock-in mouse with a hemagglutinin (HA) tag at the N-terminus of VMAT2 (Figure 1A)[39]. HA-VMAT2 signal detected via anti-HA antibodies is present

in the cell bodies of dopamine, norepinephrine and serotonin neurons (Figure S1A, S1C-D) as well as in the axonal projections of monoamine neurons in the striatum (Figure 1A, S1B). In cultured neurons, HA-VMAT2 displays punctate signal in the processes of TH-positive neurons (Figure S1E). Epitope-tagged VMAT2 is therefore faithfully targeted to neurotransmitter release sites in monoamine neurons.

To isolate the vesicle populations from the HA-VMAT2 KI mice, we used a standard differential centrifugation procedure to extract synaptic vesicles from synaptosomes via osmotic lysis (Figure 1B)[30,40]. However, since VMAT2 SVs in dopamine neurons are reported to localize in non-synaptic sites that may be excluded from synaptosomes[41], we also collected light membranes released from axonal fragments contained in the supernatant of the P2 synaptosome pellet (Figure 1B). SVs were further purified using a 5-25% glycerol gradient where the HA-VMAT2 peak appeared in fractions corresponding to SV proteins (Figure 1C). Both VGLUT2 and HA-VMAT2 signal peaks were detected in similar fractions in LP2 and P4 samples (Figure 1C). However, we do observe a shift in HA-VMAT2 signal towards lower fractions compared to VGLUT2, which is consistent with recent reports of larger SVs in dopamine neurons[42] (Figure 1C). VMAT2 and VGLUT2 SVs were then immunoisolated from gradient purified SVs using antibodies against VGLUT2 or the HA tag in VMAT2 (Figure 1D). Both HA-VMAT2 and VGLUT2 showed significant enrichment in SV populations isolated using their respective antibodies (Figure 1E).

To compare the protein composition of the two SV populations, we performed mass spectrometry with isotopic labeling by tandem mass tags (TMT). We initially completed this experiment in whole brain samples, which contain VMAT2 vesicles from all monoamine projections. Mass spectrometry of these samples indicates that many classical SV proteins were more abundant in the VGLUT2$^+$ vesicle population while VMAT2$^+$ SVs were enriched in orphan transporter Slc10A4, which is expressed by cholinergic and aminergic neurons and has a role in dopamine homeostasis[43] , and in dopamine β-hydroxylase (DBH), a luminal SV enzyme that converts dopamine into norepinephrine (Figure 1F). We also found the enrichment of VGLUT3 in monoamine vesicles, which is consistent with the presence of this glutamate transporter in serotonin neurons where it mediates glutamate corelease[44]. While the detection of DBH and Slc10A4 support the enrichment of monoamine vesicles by VMAT2 immunoisolation, many novel proteins that showed enrichment in these vesicles, as well as VMAT2 itself, were detected in only a subset of samples (Figure 1F). This presumably reflected the insufficient enrichment of this SV population from a sample where monoamine vesicles are relatively sparse. We therefore repeated the immunoisolation and subsequent analysis using striatal samples where the VMAT2$^+$ SVs are

more abundant due to the dense dopaminergic projection. Similarly to the whole brain, we find that many canonical SV proteins that are thought to be ubiquitously expressed in all SVs, show enrichment in VGLUT2 vesicles (summarized in Figure 1G-I). VGLUT2-enriched proteins include neuroprotective chaperone cysteine string protein α (CSPα), the synaptophysin family (synaptophysin, synaptogyrin1 and synaptoporin), as well as SCAMP4 and 5. We also find that members of the synaptotagmin (syt) protein family, which includes the fast SV calcium sensors syt1 and syt2, differ in abundance in the two SV populations. Specifically, VGLUT2+ SVs appear enriched in the fast calcium sensor syt2 and in calcium insensitive syt12 that has been implicated in a protein kinase A-dependent form of long-term presynaptic plasticity[45–47]. The analysis of striatal samples also revealed more proteins with high abundance in VMAT2+ SVs. These include inhibitory SNARE proteins tomosyn-1 and -2 (stxbp5 and stxbp5l) that were shown to increase the barrier for SV fusion, thereby lowering release probability[48,49]. We also find that VMAT2 vesicles contain more of chaperone DNAJb6 that is implicated in protection against α-synuclein pathology[50,51] and in juvenile-onset parkinsonism[52] as well as SCAMP2 that was shown to influence trafficking of the dopamine transporter[53]. While many well-known SV proteins differ in localization to the two vesicle populations, essential components of the release machinery such as VAMP2, SNAP25 and NSF are present at comparable levels in VMAT2$^+$ and VGLUT2$^+$ SVs (Figure 1F, 1G). Similarly, subunits of the *v*-ATPase show no consistent enrichment in either vesicle population in striatal samples (Figure S2A).

In addition to classical SV proteins, we find the differential expression of several Rab proteins, with Rab3 and Rab11b enriched in VGLUT2$^+$ SVs and Rab4 in the VMAT2$^+$ sample, which could reflect trafficking of the two transporters via distinct endosomal compartments (Figure 1F, 1G). Furthermore, we observe the more abundant association of VMAT2$^+$ SVs with dynactin and dynein subunits, suggesting a differential requirement for retrograde axonal and anterograde dendritic transport that would be consistent with the known release of monoamines from dendrites as well as axons (Figure 1F, 1G)[54]. Since VMAT2 and VGLUT2 vesicles differ in reliance on adaptor protein complexes for recycling from the plasma membrane, we also analyzed the data for AP-2 and AP-3 subunit abundance in the two SV populations (Figure S2B). While AP-2 subunits are present at comparable levels in both vesicle populations, AP-3 components are detected consistently only in whole brain samples where they associate preferentially with VMAT2 vesicles.

Expression of SV proteins in primary dopamine and glutamate neurons. To assess differences in VMAT2$^+$ and VGLUT2$^+$ SV composition, we first used primary midbrain cultures

from HA-VMAT2 KI mice as these cultures contain both dopamine neurons and VGLUT2$^+$ glutamate neurons. To compare SV protein abundance in these neuronal populations, we identified regions of interest (ROIs) based on the expression of HA-VMAT2 or VGLUT2 and quantified the fluorescence intensity of candidate proteins in both sets of ROIs. Since VMAT2 localizes to the somatodendritic as well as axonal compartment[55], we also examined the colocalization of HA-VMAT2 with the dendritic protein MAP2. We find a more diffuse HA-VMAT2 signal in MAP2$^+$ fibers, while the vast majority of bright punctate structures similar in size and appearance to VGLUT2$^+$ varicosities localize to MAP2$^-$ axonal projections (Figure S3). These results therefore compare axonal varicosities from the two neuronal populations. As predicted by the proteomics results, orphan transporter Slc10A4[43] localizes to VMAT2$^+$ rather than VGLUT2$^+$ terminals (Figure 2A). In contrast, VGLUT2$^+$ sites contain more of the canonical SV protein synaptophysin (Figure 2E, S4A) as well as the related synaptogyrin1 (Figure 2F, S4B). VGLUT2$^+$ terminals also contain more of presynaptic chaperone CSPα (Figure 2D) and SCAMP5 (Figure 2G, S4C). However, the SV SNARE protein VAMP2 occurs at similar levels in both release sites (Figure 2H, S4D) supporting the specificity of differences for other proteins and arguing against substantial differences in SV cluster size. For synaptophysin, synaptogyrin1, CSPα, SCAMP5 and Slc10A4, the same trends in expression were consistently observed in all analyzed dopamine and glutamate neurons, including fields of view that contain both dopamine and VGLUT2$^+$ glutamate neurons. However, the analysis of syt2 revealed that although syt2 signal in dopamine neurons was consistently close to background, glutamate neurons fall into two populations: VGLUT2 neurons with low or nonexistent syt2 signal similar to dopamine neurons, and another with strong syt2 expression that colocalizes with VGLUT2 (Figure 2C, 2I, 2J). These findings suggest a molecular heterogeneity among the VGLUT2$^+$ glutamate neurons present in midbrain cultures. The other fast calcium sensor syt1 occurs in both types of neurons, but its signal intensity in midbrain cultures is consistently higher at dopamine release sites (Figure 2B).

To directly test whether dopamine and glutamate release sites differ in the copy number of SV proteins, we quantified both VMAT2-enriched syt1 and VGLUT2-enriched CSPα in the same ROIs (Figure 2K-N, S5). The ratio of syt1/CSPα is significantly higher in VMAT2$^+$ varicosities indicating that individual dopamine release sites contain more syt1 and less CSPα than VGLUT2 terminals (Figure 2M, 3N). These results support the differences in SV composition identified by mass spectrometry and show that possible differences in SV cluster size in dopamine versus glutamate neurons[42] cannot alone explain differences in SV protein abundance in VGLUT2 versus VMAT2 release sites.

The composition of synaptic vesicles differs at dopamine and glutamate release sites in the striatum. To test the differential expression of SV proteins at dopamine and glutamate release sites within the intact neural circuitry, we stained for candidate proteins in brain slices from HA-VMAT2 KI mice and quantified their abundance in VMAT2$^+$ and VGLUT2$^+$ varicosities (Figure 3, Figure S6). We focused on the striatum since it receives both dense dopamine projections from the midbrain and VGLUT2$^+$ input from the thalamus. We acquired z-stacks and used automatic segmentation to generate three-dimensional (3D) VGLUT2 and VMAT2 surfaces followed by quantification of the mean fluorescence intensity for the proteins of interest within the same image (Figure 3A). As predicted by the proteomics results and confirmed in primary culture, Slc10A4 is enriched at dopamine release sites and colocalizes with VMAT2 (Figure 3B, 3C). If combined with TH staining to differentiate dopamine release sites from cholinergic terminals, which also express this transporter[56], Slc10A4 can serve as a reliable marker for dopamine release sites. CSPα (Figure 3D, 3E), SCAMP5 (Figure S6A, S6B) and synaptophysin (Figure S6C, S6D) are more abundant in VGLUT2$^+$ varicosities. As in primary cultures, the mean intensity of VAMP2 signal was comparable in VGLUT2$^+$ and VMAT2$^+$ surfaces (Figure S6E, S6F).

Experiments in primary cultures indicated that syt2 is present in only a subset of VGLUT2$^+$ neurons (Figure 2I). We stained for syt2 in multiple brain regions that receive VGLUT2$^+$ projections to determine whether VGLUT2$^+$ glutamate neurons in different structures differ in expression of syt2 (Figure 4). We focused on the striatum, CA2 region of the hippocampus, and the posterior thalamic nucleus (PO), dorsal lateral geniculate nucleus (DLG) and ventral posterior nucleus (VPN)[57]. We observed HA-VMAT2$^+$ fibers in all these structures, enabling us to compare the fraction of VMAT2$^+$ and VGLUT2$^+$ varicosities that contain syt2 as well as to compare syt2 intensity at the two classes of release site. VMAT2$^+$ and VGLUT2$^+$ varicosities were considered syt2$^+$ if 40% of their volume overlapped with syt2 labeling (Figure 4A). Since none of the three presynaptic proteins are expressed by all neurons, the labeling density in all brain regions was sufficiently low to assess the extent of overlap without significant contribution of signal from adjacent structures (Figure 4B, 4C). We find that although syt2 signal is very low in VGLUT2$^+$ terminals of the striatum and in region CA2 of the hippocampus, it is abundant at the majority of VGLUT2$^+$ release sites in thalamic nuclei and absent from the majority of VMAT2$^+$ varicosities in all structures (Figure 4B-D). When we quantified the mean intensity of syt2 signal in monoamine and glutamate release sites across all regions, we find that this calcium sensor is significantly more abundant in VGLUT2 varicosities in the DLG that contains the large VGLUT2$^+$ terminals of retinal ganglion cells[58] (Figure 4B, 4C, 4E) and in the VPN where VGLUT2-dependent glutamate

release relays sensory information from the spinal cord and brain stem[59] (Figure 4E). Syt2 abundance was not significantly different in the striatum, CA2 and PO. These results confirm the differences in composition of VMAT2$^+$ and VGLUT2$^+$ SVs identified by the proteomics.

SV protein composition of VGLUT2+ release sites in dopamine neurons differs from VMAT2-only varicosities. The corelease of glutamate by midbrain dopamine neurons raises the question whether SVs at dopamine and glutamate release sites differ within the same population of neurons. We previously found that the exocytosis and recycling of VGLUT2$^+$ SVs in cultured dopamine neurons occurs with faster kinetics than VMAT2$^+$ SVs[22], indicating differences in the mode of release in the same cell. Glutamate release from coreleasing neurons also differs from dopamine release in short-term plasticity[22]. If VGLUT2$^+$ and VMAT2$^+$ SVs in dopamine neurons indeed differ in protein content, it should result in altered presynaptic composition in VGLUT2+ release sites in dopamine neurons.

The corelease of glutamate with dopamine reflects the expression of VGLUT2 by a subset of midbrain dopamine neurons[32,33]**.** To investigate the localization of VMAT2 and VGLUT2 in these cells, we again took advantage of midbrain cultures from HA-VMAT2 mice (Figure 5). We find that within TH$^+$ neurons that label for both VMAT2 and VGUT2, most release sites contain detectable signal for both transporters, even though the relative intensities vary (Figure 5A-C). While VMAT2 signal is comparable in release sites of VMAT2-only and VMAT2$^+$/VGLUT2$^+$ neurons, VGLUT2 abundance in presynaptic varicosities of cultured VMAT2$^+$/VGLUT2$^+$ neurons is significantly lower than in glutamate-only cells (Figure 5D). This suggests a lower VGLUT2 copy number per vesicle or its presence on a subset of vesicles within the coreleasing terminals.

We also determined whether VMAT2$^+$/VGLUT2$^+$ sites differ from VMAT2-only varicosities in the expression of other SV proteins. We find that VMAT2-enriched Slc10A4 and equally distributed VAMP2 are present at similar levels in VMAT2-only and VMAT2$^+$/VGLUT2$^+$ boutons (Figure 5G-H). Likewise, the abundance of SV calcium sensors syt1 and syt2 is not affected by the presence of VGLUT2 at VMAT2 sites (Figure 5I-J). However, CSPα, SCAMP5 and synaptophysin are significantly more abundant at VMAT2+/VGLUT2+ boutons compared to VMAT2-only SV clusters (Figure 5E, 5F, 5K-M). Furthermore, we find that the abundance of Slc10A4 measured in individual release sites of coreleasing neurons correlates better with VMAT2 than VGLUT2 abundance at the same varicosities (Figure 5N). Conversely, synaptophysin signal correlates with VGLUT2 expression (Figure 5O) supporting the preferential targeting of synaptophysin to VGLUT2 SVs. Altogether, we find that VGLUT2$^+$ presynaptic varicosities in dopamine neurons

resemble typical glutamate release sites pointing to a distinct composition of VGLUT2 SVs within dopamine neurons.

SVs containing VGLUT2 and VMAT2 segregate within presynaptic varicosities of dopamine/glutamate coreleasing neurons. VMAT2 and VGLUT2 colocalize at the majority of release sites made by cultured dopamine neurons, but previous work using heterologous reporters has suggested that they may localize to distinct SVs at these sites[22]. We have now addressed this question using endogenous proteins. Since classical confocal microscopy does not allow us to resolve SVs within a single presynaptic bouton, we thus took advantage of the Nikon Spatial Array Confocal (NSPARC) technology to access enhanced spatial resolution compared to classical confocal detection systems[60]. We focused on individual presynaptic varicosities that contain TH, HA-VMAT2 and VGLUT2 to evaluate the degree of colocalization between VMAT2 and VGLUT2 signal within the release site and to investigate the colocalization of the signal for the transporters and differentially expressed SV proteins (Figure 6). First, we compared the colocalization of HA-VMAT2 and VGLUT2 (Figure 6B, 6C), using HA signal stained with two secondary antibodies coupled to different fluorophores as control (Figure 6A). As expected, HA signal detected in two channels shows a high degree of colocalization. We also detect substantial overlap between HA-VMAT2 and VGLUT2 signal, however, it is significantly lower compared to the control condition comparing HA signal in two channels (Figure 6A). Since we detect a partial segregation of VMAT2 and VGLUT2 into different structures within presynaptic varicosities, we compared the correlation of VGLUT2-enriched synaptophysin and VMAT2-enriched syt1 with the signal for the two transporters. We find that synaptophysin fluorescence correlates more with VGLUT2 than VMAT2 in presynaptic terminals that contain both transporters (Figure 6B) while syt1 signal displays similar correlation with both VGLUT2 and VMAT2 (Figure 6C). These results suggest that VGLUT2 targets to an SV population with distinct composition.

Loss of SCAMP5 selectively impairs the synaptic recycling of VGLUT2 vesicles. If VGLUT2 and VMAT2 SVs differ in composition even in the same neuronal population, then elimination of a differentially expressed protein should preferentially affect the synaptic recycling of vesicles expressing more of that protein. We focused on SCAMP5 as we have validated its significantly higher abundance on VGLUT2 vesicles and previous studies have shown that its loss of function affects the SV cycle and NT release[61,62]. To address its role in the release of VMAT2$^+$ versus VGLUT2$^+$ vesicles, we took advantage of the pHluorin reporter that enables monitoring the properties of the SV cycle when fused to luminal domains of SV proteins. PHluorin fluorescence is quenched in resting, acidic SVs but increases as SV fusion exposes the vesicle lumen to the

neutral extracellular environment and decreases with endocytosis and vesicle reacidification[63]. We have previously shown that pHluorin-tagged VMAT2 reliably targets to AP-3-dependent SVs in both dopamine and hippocampal neurons whereas VGLUT2-pHluorin is excluded from these vesicles[22,27]. To test whether the elimination of SCAMP5 has differential effects on these SV pools, we used shRNA to knock down (KD) SCAMP5 expression (Figure 7). Lentiviral delivery of a KD construct targeting SCAMP5 results in an efficient elimination of the SCAMP5 protein from hippocampal neurons without affecting neuronal morphology or the abundance of the SV calcium sensor syt1 (Figure 7A). To test the role of SCAMP5 in the VGLUT2$^+$ SV population, we infected neuronal cultures with VGLUT2-pHluorin together with a control scrambled construct or SCAMP5 KD alone or in combination with an shRNA resistant rescue construct. Neurons were stimulated for 60 seconds at 10 Hz. We find that the recycling of VGLUT2 SVs is reduced in the KD condition compared to a scrambled control but is restored to control levels if SCAMP5 expression is rescued in the KD background (Figure 7B). The synaptic recycling of AP-3-dependent SVs targeted by VMAT2-pHluorin is however not affected by the loss of SCAMP5 (Figure 7C). These findings indicate that SCAMP5 is specifically involved in recycling of vesicles that are enriched in VGLUT2 and despite its high abundance in the cell type, does not have a detectable effect on the trafficking of the SV population targeted by VMAT2. Since the loss of AP-3 does not completely abolish VMAT2 recycling[27], it remains possible that AP-3-independent VMAT2$^+$ vesicles depend on SCAMP5 function but this effect is not detected due to the abundance of VMAT2 on AP-3 SVs.

DISCUSSION

In this study we compared the proteome of two classes of synaptic vesicles that differ in reliance on biogenesis pathways and responsiveness to neuronal firing frequency. We find that synaptic vesicles that store monoamine transmitters differ substantially in protein composition compared to VGLUT2-positive glutamate vesicles, with lower abundance of many canonical SV proteins and enrichment in others. These findings add to growing evidence of diversity in presynaptic composition and function among neuronal populations[5,16,24,26]. Specifically, we bring evidence of differences in the SV proteome across neurotransmitter systems with corresponding distinct regulation of release.

Addressing diversity in presynaptic composition and function. Multiple studies have used proteomics approaches to address the diversity of presynaptic composition across neuronal populations[16] or to specifically investigate the unique features of dopamine release machinery[64,65]. These studies relied on synaptosomes sorted based on cell type specific expression of

fluorescent proteins[16,64,66] or proximity labeling approaches[26,65]. Despite differences in methodology, some SV proteins emerge repeatedly from our study as well as from previous work as enriched components of the dopamine release machinery. These include Slc10A4[16,64,65], VAT1[16,64] , SV2c[16,64]. The enrichment of dynactin subunits in dopamine synaptosomes[16] is also compatible with our finding that dynactin and dynein are associated to a higher extent with VMAT2 compared to VGLUT2 vesicles, possibly indicating the importance of axonal transport in dopamine release site biology. Conversely, while syt7[65] and -17[64,65] were previously identified as proteins enriched in dopamine release sites, we do not find their significant enrichment in VMAT2 vesicles. This could however be explained by the reported targeting of syt7 to the plasma membrane, which would explain its abundance in dopamine synaptosomes but not SVs[67]. Functional data also supports the localization of syt17 on endosomal organelles that differ from SVs[68,69]. Importantly, distinct pattern of canonical SV proteins in dopamine vesicles did not emerge from previous work. By comparing VMAT2 vesicles directly to another SV population with distinct functional properties, we are able to access information about differences in the abundance of ubiquitously expressed SV components. Our approach reveals both enriched and de-enriched examples among SV proteins that are thought to be present throughout synaptic vesicles across cell types. For example, synaptophysin – a widely used presynaptic marker – and related synaptogyrin1 and synaptoporin are all present at lower levels on monoamine vesicles. SCAMP and synaptotagmin protein families are represented by different isoforms in the two vesicle populations and neuroprotective chaperone CSPα is less abundant in VMAT2 SVs. Our findings therefore reveal substantial differences in the composition of SVs that store the modulatory monoamine transmitters compared to the fast synaptic transmitter glutamate.

Functional implications of differential SV composition. While some differentially expressed proteins are largely absent from one SV population (Slc10A4), others differ in the expressed isoform of a protein family (synaptotagmins, SCAMPs), and many differ in abundance (Figure 1). While altered copy number of most SV proteins does not typically lead to severe impairments in NT release[70,71], the combined effect of reduced abundance of multiple SV proteins or altered SV protein stoichiometry is not known. Furthermore, while initially benign, reduced expression of SV proteins CSPα and SV2 can lead to impaired synaptic function over time[72,73]. These observations suggest that the copy number of some SV proteins may be critical for long term maintenance of synaptic function and diversity in abundance may have links to selective vulnerability of some synapse types over aging. The low expression of CSPα in dopamine neurons is especially interesting since the loss of function of this SV-localized chaperone leads to presynaptic

degeneration[71]. Furthermore, CSPα and α-synuclein cooperate with each other in assuring presynaptic integrity[74] and recent evidence also suggests that increased CSPα expression reduces aggregation of mutant synuclein in a mouse model of Parkinson's disease[75].

In addition to potential impact on synapse stability and maintenance, variations in the abundance or isoform of SV proteins could influence the dynamics of SV exo- and endocytosis as well as the plasticity of neurotransmitter release. For instance, several studies have investigated functional differences between syt1 and syt2 with some reporting distinct kinetics of neurotransmitter release mediated by the two calcium sensors[47,76], though not all studies have observed this effect[77]. While the primary function of synaptophysins and -gyrins is less clear, loss of these proteins affects the trafficking of other SV components[78–80] as well as short-term plasticity of neurotransmission[81,82]. Among the SCAMP family, SCAMP5 is the best studied in the context of neurotransmitter release with reports of impaired glutamate release and effects on axonal trafficking and release site clearance[61,62,83]. Research on SCAMPs in dense core vesicle exocytosis suggests that these proteins have distinct effects on fusion events and their differential presence on VMAT2 and VGLUT2 SVs could therefore affect the properties of monoamine and glutamate release[84]. Furthermore, findings that SCAMP2 affects the trafficking of the dopamine transporter DAT and serotonin transporter SERT support its importance in monoamine release sites[53,85]. Our results support a specific role for SCAMP5 in vesicles that are targeted by VGLUT2 (Figure 7) and reinforce the notion that differences in SV composition between VMAT2 and VGLUT2 vesicles confer differences in the regulation of monoamine and glutamate release.

Presynaptic composition in dopamine/glutamate coreleasing neurons. Our previous findings support the differential regulation of dopamine and glutamate release from coreleasing neurons via packaging into functionally distinct vesicles[22]. However, glutamate corelease was also shown to affect dopamine packaging into SVs via vesicular synergy, which would require at least a partial coexistence of VMAT2 and VGLUT2 on the same vesicle[32]. In the present study, we find that HA-VMAT2 and VGLUT2 colocalize in most presynaptic varicosities in cultured dopamine/glutamate coreleasing neurons but often differ in abundance. Previous work that used cultures of FACS sorted dopamine neurons or human IPSC derived dopamine cells have reported release sites that contain only VGLUT2 or VMAT2 signal with VGLUT2 segregating even from TH[86–88]. We do find TH-negative VGLUT2 release sites in the vicinity of coreleasing neurons, but our midbrain cultures also contain VGLUT2-positive glutamate-only neurons. Since we could not conclusively differentiate VGLUT2-only dopamine neuron varicosities from glutamate neuron terminals, we included only VGLUT2/VMAT2 co-expressing sites in our analysis. An increase in

the abundance of some VGLUT2 vesicle enriched proteins in these sites suggests that these proteins are part of the core machinery for glutamate release. Super-resolution and live imaging analysis further indicates that distinct composition drives the functional differences between vesicle pools targeted by VMAT2 and VGLUT2 (Figures 6 and 7).

In striatal tissue that receives dense dopamine projections, colocalization of VGLUT2 with dopamine release site markers appears very low[41,87,89,90]. This is true even in the nucleus accumbens medial shell where functional evidence supports glutamate release from dopamine neurons and intersectional labeling approaches indicate that most dopamine axons originate from coreleasing cells[34,91–93]. This could be partially due to the lower abundance of VGLUT2 in DA terminals compared to glutamate neurons (Figure 5D) which makes it challenging to differentiate dopamine neuron VGLUT2 signal from background in densely packed brain tissue. Several studies have however also reported that VGLUT2/VMAT2 segregation is enhanced by contact with striatal neurons[87,94] and may therefore be more prominent in a network with preserved connectivity[41]. Further analysis is needed to determine whether dopamine neuron glutamate release sites are more likely to contain the sparse active zones observed in dopamine axonal varicosities[24,25,95] and whether SV proteins like synaptophysin or SCAMP5 differ in abundance in VMAT2 and VGLUT2 varicosities if the transporters indeed segregate into distinct release sites within the same neuron.

Mechanism for generating diversity in SV composition. It is well established that neuronal populations differ in transcriptional profile[13–15], which likely contributes to the diversity in presynaptic composition. Indeed, some SV proteins like Slc10A4 and syt2 display differences in RNA abundance between monoamine and VGLUT2-positive glutamate neurons[14]. RNAs coding for synaptophysin, SCAMP5 and other SV proteins, but also dynactin and active zone components RIM1 and bassoon are however abundant across neuronal populations[14]. This points to differences in post-transcriptional processes like protein turnover in establishing the distinct composition of monoamine and glutamate SVs and release sites. Furthermore, we find that differentially expressed SV proteins can display preferential colocalization with either VGLUT2 or VMAT2 within the same neuron and presynaptic varicosity (Figures 5 and 6). Similar observations were made in COS7 cells, showing enrichment of VMAT2 and some classical SV proteins, specifically synaptophysin, in distinct populations of vesicles within the same cell[86]. These findings indicate that differential dependence on intracellular protein trafficking mechanisms likely contribute to the observed differences in protein composition between VMAT2 and VGLUT2 vesicles. Indeed, the reliance of VMAT2 and VGLUT2 on distinct SV replenishment pathways is

likely involved in establishing distinct protein composition between these SV populations[12,22,27]. A previous analysis of whole brain SV composition in WT versus AP-3 KO mice confirmed previously known AP-3 client proteins, including VAMP7 and identified new SV proteins that depend on AP-3 function, including phospholipid flippase ATP8a1 and Slc35g2 – a transporter with unknown function[30,96,97]. While the abundance of most classical SV proteins was not found to be changed[30], in most synapses, AP-3-dependent vesicles only constitute a small fraction of the total SV pool[31,98] making it challenging to detect potential changes in the abundance of ubiquitous SV proteins that may differ in preference for sorting pathway. Surprisingly, while our data indicates that Slc35g2 is more abundant in VMAT2 SVs, VAMP7 and ATP8A1 do not seem to be differentially enriched in the two vesicle populations (Figure 1F, 1G). More work is therefore needed to clarify whether the AP-3-dependent proteins VAMP7 and VMAT2 indeed target to the same pool of SVs or reside in separate populations of vesicles within the nerve terminal[99]. Among proteins enriched in VGLUT2-positive SVs, synaptophysin has been shown to not depend on AP-3[97,100] and SCAMP5 is known to interact with AP-2[62]. We do find both synaptophysin and SCAMP5 in dopamine release sites, but these terminals likely also contain AP-3-independent SVs, since dopamine release is not completely abolished in the absence of AP-3[27]. Use of recently developed cell type specific proteomics strategies may help to clarify the contribution of adaptor protein complexes in SV protein sorting in dopamine neurons and other neuronal populations[26,65,101]. It also remains to be determined whether VMAT2 and VGLUT2 colocalize on the AP-3-indepenent SV pool, which could be the source vesicular synergy observed between the two transmitters[32].

In summary, we elucidate the distinct molecular identity of monoamine and VGLUT2$^+$ glutamate SVs that differ in biogenesis mechanism and responsiveness to neuronal firing frequency. SCAMP5 example illustrates the diverse composition and regulation of these vesicle pools even in the same neuronal population. Other differentially expressed SV proteins likely cooperate in determining the distinct functional features of VMAT2$^+$ and VGLUT2$^+$ vesicles.

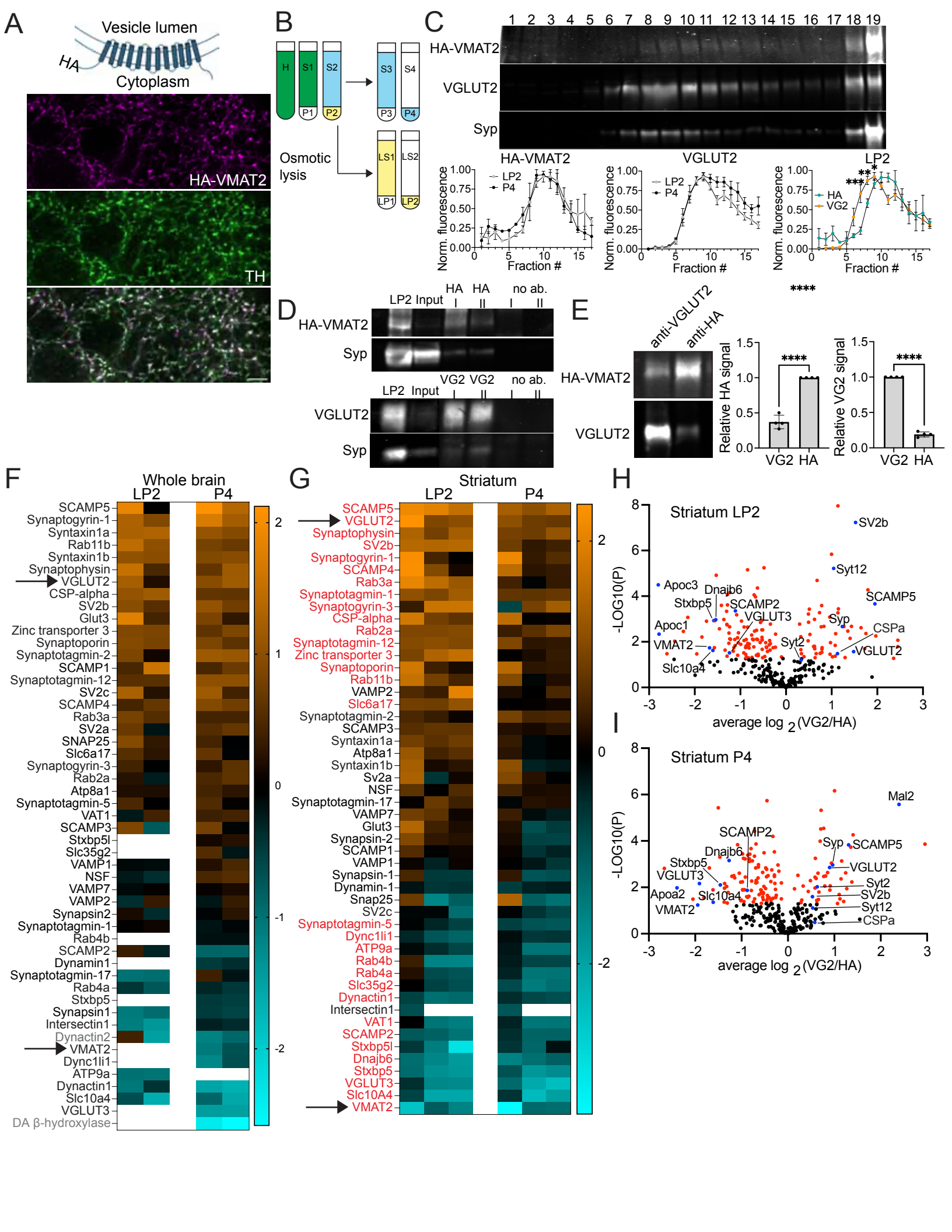
A
Vesicle lumen
HA
Cytoplasm
HA-VMAT2
TH
B
H
S1
S2
S3
S4
P1
P2
P3
P4
Osmotic lysis
LS1
LS2
LP1
LP2
C
1 2 3 4 5 6 7 8 9 10 11 12 13 14 15 16 17 18 19
HA-VMAT2
VGLUT2
Syp
HA-VMAT2
VGLUT2
LP2
LP2
P4
HA
VG2
Norm. fluorescence
Fraction #
D
LP2 Input
HA I
HA II
no ab. I
no ab. II
HA-VMAT2
Syp
VG2 I
VG2 II
VGLUT2
E
anti-VGLUT2
anti-HA
HA-VMAT2
VGLUT2
Relative HA signal
Relative VG2 signal
****
VG2
HA
F
Whole brain
LP2
P4
SCAMP5
Synaptogyrin-1
Syntaxin1a
Rab11b
Syntaxin1b
Synaptophysin
VGLUT2
CSP-alpha
SV2b
Glut3
Zinc transporter 3
Synaptoporin
Synaptotagmin-2
SCAMP1
Synaptotagmin-12
SV2c
SCAMP4
Rab3a
SV2a
SNAP25
Slc6a17
Synaptogyrin-3
Rab2a
Atp8a1
Synaptotagmin-5
VAT1
SCAMP3
Stxbp5l
Slc35g2
VAMP1
NSF
VAMP7
VAMP2
Synapsin2
Synaptotagmin-1
Rab4b
SCAMP2
Dynamin1
Synaptotagmin-17
Rab4a
Stxbp5
Synapsin1
Intersectin1
Dynactin2
VMAT2
Dync1li1
ATP9a
Dynactin1
Slc10a4
VGLUT3
DA β-hydroxylase
G
Striatum
LP2
P4
SCAMP5
VGLUT2
Synaptophysin
SV2b
Synaptogyrin-1
SCAMP4
Rab3a
Synaptotagmin-1
Synaptogyrin-3
CSP-alpha
Rab2a
Synaptotagmin-12
Zinc transporter 3
Synaptoporin
Rab11b
VAMP2
Slc6a17
Synaptotagmin-2
SCAMP3
Syntaxin1a
Atp8a1
Syntaxin1b
Sv2a
NSF
Synaptotagmin-17
VAMP7
Glut3
Synapsin-2
SCAMP1
VAMP1
Synapsin-1
Dynamin-1
Snap25
SV2c
Synaptotagmin-5
Dync1li1
ATP9a
Rab4b
Rab4a
Slc35g2
Dynactin1
Intersectin1
VAT1
SCAMP2
Stxbp5l
Dnajb6
Stxbp5
VGLUT3
Slc10A4
VMAT2
H
Striatum LP2
-LOG10(P)
average log 2 (VG2/HA)
SV2b
Syt12
Apoc3
Dnajb6
Stxbp5
SCAMP2
VGLUT3
SCAMP5
Syp
CSPa
Apoc1
VMAT2
Syt2
VGLUT2
Slc10a4
I
Striatum P4
Mal2
SCAMP2
Syp
SCAMP5
Dnajb6
Stxbp5
VGLUT2
VGLUT3
Syt2
Apoa2
Slc10a4
SV2b
VMAT2
Syt12
CSPa

Figure 1. Isolation and proteomic profiling of VMAT2$^+$ and VGLUT2$^+$ SVs.

A. We used CRISPR to generate a knock-in mouse with an HA tag in the cytoplasmic N-terminus of VMAT2. Confocal image of the striatum stained for HA and TH shows HA-VMAT2 signal in TH-positive axonal fibers. Scale bar = 5 µm.

B. Scheme of the protocol for isolating synaptic vesicles. Synaptosomes from P2 pellet fraction were subjected to osmotic lysis to release synaptic vesicles from presynaptic terminals. Released vesicles (LS1) were separated from synaptic plasma membranes (LP1) and then sedimented in the LP2 pellet. In parallel, we collected light organelles from supernatant S2 to isolate axonal vesicles that were not concentrated in varicosities (P4). Fractions highlighted in color were used in the following steps.

C. Western blot of HA-VMAT2, VGLUT2 and synaptophysin signal in LP2 samples loaded on a 5-25% glycerol gradient. 10 µL of a 500 µL fraction was loaded per lane.

Graphs show the comparison of mean HA-VMAT2 and VGLUT2 signal intensities in gradient fractions of LP2 and P4 samples and the comparison of HA-VMAT2 versus VGLUT2 signal in LP2 samples quantified on dot blots. Data indicate mean ± SEM. * < 0.05, ** < 0.001, *** <0.001, by unpaired t-test

D. Immunoblots showing HA-VMAT2 and synaptophysin (left) or VGLUT2 and synaptophysin (right) in LP2, starting material for vesicle isolation (LP2 after gradient purification and dialysis) and on Dynabeads with antibody used for isolation or in a negative control where antibody was not added.

E. Immunoblots and quantification of HA-VMAT2 and VGLUT2 signal in vesicles immunoisolated using anti-VGLUT2 or anti-HA antibodies. Data indicate mean ± SEM. **** <0.0001, by unpaired t-test

F. Examples of proteins quantified on VMAT2 and VGLUT2 SVs isolated from whole brain samples from HA-VMAT2 KI mice. Data was normalized to the amount of total protein in each sample and is presented as a heat map of log2 values of VGLUT2/VMAT2 ratio. Each column represents an independent experiment. Proteins indicated in gray are not detected in samples from the striatum.

G. Examples of proteins quantified on VMAT2 and VGLUT2 SVs isolated from striatal samples of HA-VMAT2 KI mice. Data was normalized to the amount of total protein in each sample and is presented as a heat map of log2 values of VGLUT2/VMAT2 ratio. Each column represents an independent experiment. Proteins highlighted in red show significant enrichment in one SV population ($P < 0.05$) and have a VGLUT2/VMAT2 ratio above 1.5 or below -1.5.

H-I. Volcano plots showing protein abundance in VMAT2 versus VGLUT2 SVs in striatal LP2 (H) and P4 samples (I) as determined by TMT labeling and mass spectrometry. Data was analyzed in three independent experiments. Data points highlighted in red have p-values < 0.05. Blue data points are associated with labels.

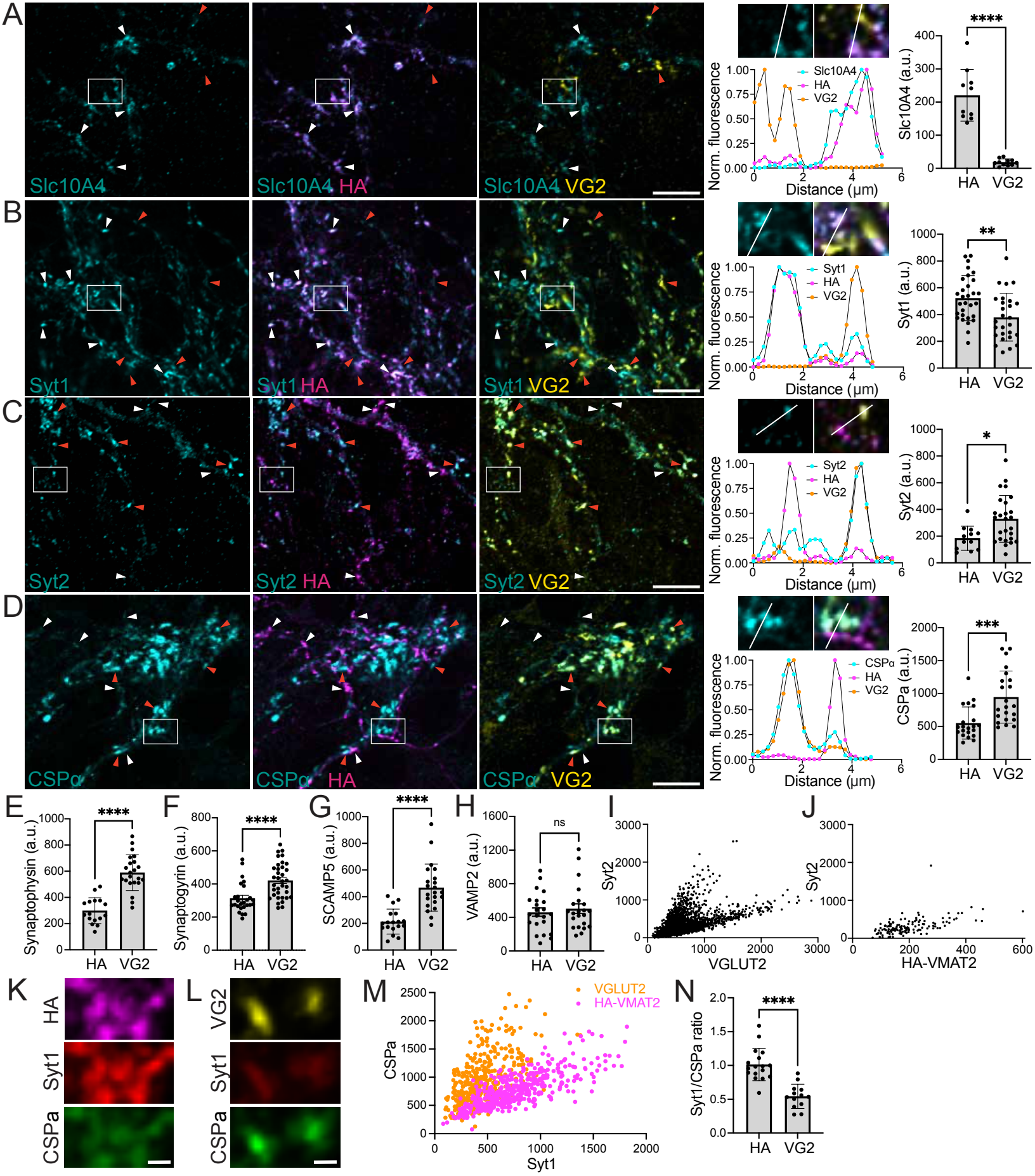
A
Slc10A4
Slc10A4 HA
Slc10A4 VG2
Norm. fluorescence
Distance (μm)
Slc10A4
HA
VG2
Slc10A4 (a.u.)
****
B
Syt1
Syt1 HA
Syt1 VG2
Syt1 (a.u.)
**
C
Syt2
Syt2 HA
Syt2 VG2
Syt2 (a.u.)
*
D
CSPα
CSPα HA
CSPα VG2
CSPa (a.u.)
***
E
Synaptophysin (a.u.)
****
F
Synaptogyrin (a.u.)
****
G
SCAMP5 (a.u.)
****
H
VAMP2 (a.u.)
ns
I
Syt2
VGLUT2
J
Syt2
HA-VMAT2
K
HA
Syt1
CSPa
L
VG2
Syt1
CSPa
M
VGLUT2
HA-VMAT2
CSPa
Syt1
N
Syt1/CSPa ratio
****

Figure 2. Dopamine and glutamate release sites in primary midbrain neurons differ in composition.

A-D. Confocal images of midbrain cultures from HA-VMAT2 KI mice showing the distribution of Slc10A4 (A), syt1 (B), syt2 (C) and CSPα (D) in VMAT2 and VGLUT2 varicosities and the quantification of mean fluorescence intensity of the proteins of interest in the two types of release sites. White arrowheads point to VMAT2 and orange arrowheads to VGLUT2 varicosities. Scale bars = 10 μm. Inset shows magnification of the area indicated by the white box and a line ROI with corresponding fluorescence profiles in three channels shown below.

E-H. Quantification of mean fluorescence intensity of synaptophysin (E), synaptogyrin1 (F), SCAMP5 (G) and VAMP2 (H) in DA release sites identified as HA-VMAT2 clusters in TH+ cells and in VGLUT2-positive glutamate release sites. Each data point represents the mean intensity of the signal for proteins of interest in all ROIs per image.

I-J. Scatter plot of syt2 and VGLUT2 (I) and syt2 and HA-VMAT2 (J) fluorescence intensity in individual release sites.

K-N. Presynaptic varicosities stained for HA-VMAT2, synaptotagmin1 and CSPα (K) or VGLUT2, synaptotagmin1 and CSPα (L). Scale bar = 1 μm. Scatter plot of intensities of CSPα and syt1 signal quantified in individual HA-VMAT2 or VGLUT2 varicosities (M) and quantification of syt1/CSPα ratio averaged per image (N).

Data indicate mean ± SEM in all panels. * < 0.05, ** <0.01, *** < 0.001, **** <0.0001, by unpaired t-test (A, B, C, E, G, N), or Mann-Whitney test (D, F, H).

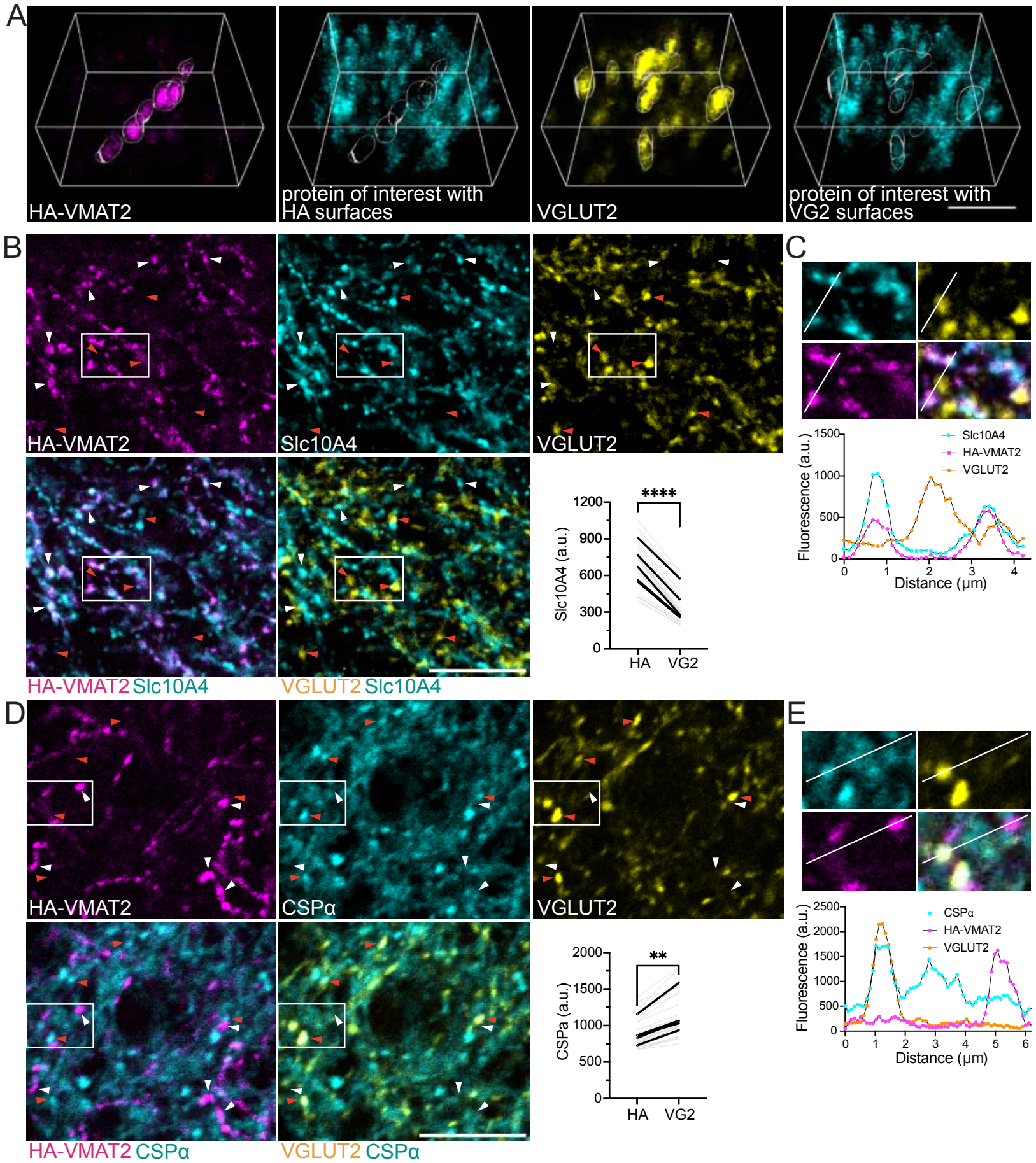
A
HA-VMAT2
protein of interest with HA surfaces
VGLUT2
protein of interest with VG2 surfaces
B
HA-VMAT2
Slc10A4
VGLUT2
HA-VMAT2 Slc10A4
VGLUT2 Slc10A4
****
Slc10A4 (a.u.)
1200
900
600
300
0
HA
VG2
C
Slc10A4
HA-VMAT2
VGLUT2
Fluorescence (a.u.)
1500
1000
500
0
0
1
2
3
4
Distance (µm)
D
HA-VMAT2
CSPα
VGLUT2
HA-VMAT2 CSPα
VGLUT2 CSPα
**
CSPa (a.u.)
2000
1500
1000
500
0
HA
VG2
E
CSPα
HA-VMAT2
VGLUT2
Fluorescence (a.u.)
2500
2000
1500
1000
500
0
0
1
2
3
4
5
6
Distance (µm)

Figure 3. Dopamine release sites and VGLUT2^{+} glutamate terminals in the striatum differ in the abundance of SV proteins.

A. Example of 3D surfaces generated in a striatal z-stack of a staining for HA-VMAT2 (magenta) or VGLUT2 (yellow). The same surfaces are transferred to the channel showing the staining for a protein of interest (cyan) for quantification of its the mean intensity in HA-VMAT2 and VGLUT2 surfaces. Scale bar = 4 µm.

B-C. B. Confocal image of a single plane in a striatal slice from a HA-VMAT2 KI mouse stained for HA-VMAT2, Slc10A4 and VGLUT2 together with quantification of mean Slc10A4 intensity in 3D surfaces generated based on HA-VMAT2 or VGLUT2 signal. Gray lines show mean values of varicosities per image, black lines indicate the mean values per mouse. **** <0.0001 by paired t-test on mouse averages. Scale bar = 10 µm. White arrowheads point to HA-VMAT2 and orange arrowheads to a VGLUT2 varicosities. C. Magnified view of the area highlighted by white box in B and plot profile of fluorescence intensities in three channels along the line ROI.

D-E. D. Confocal image of a single plane in a striatal slice from a HA-VMAT2 KI mouse stained for HA-VMAT2, CSPα and VGLUT2 together with quantification of mean CSPα intensity in 3D surfaces generated based on HA-VMAT2 or VGLUT2 signal. Gray lines show mean values of varicosities per image, black lines indicate the mean values per mouse. ** = 0.006 by paired t-test on mouse averages. Scale bar = 10 µm. White arrowheads point to HA-VMAT2 and orange arrowheads to a VGLUT2 varicosities. Magnified view of the area highlighted by white box in D and plot profile of fluorescence intensities in three channels along the line ROI.

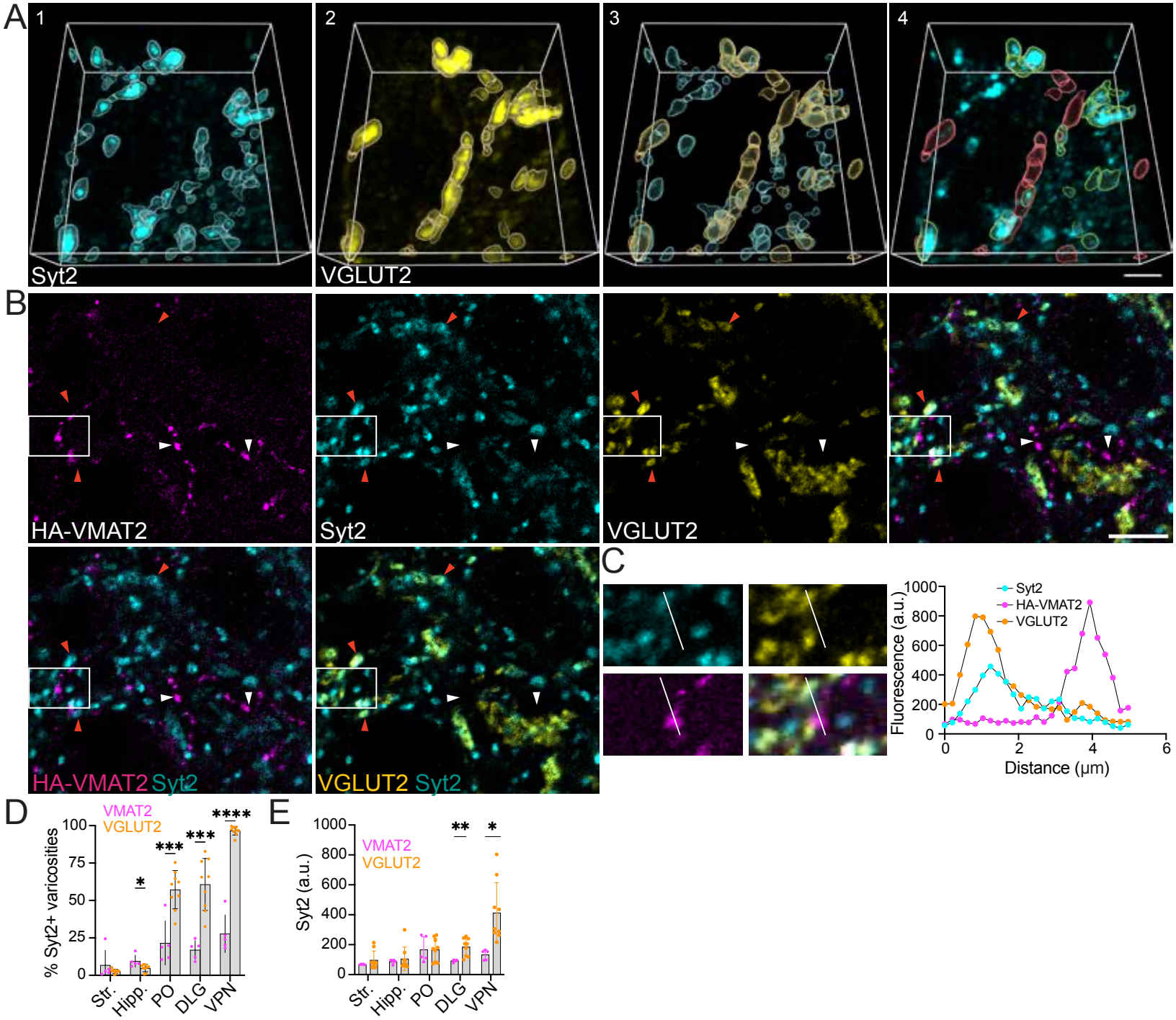
A
1
2
3
4
Syt2
VGLUT2
B
HA-VMAT2
Syt2
VGLUT2
HA-VMAT2 Syt2
VGLUT2 Syt2
C
Syt2
HA-VMAT2
VGLUT2
Fluorescence (a.u.)
Distance (µm)
D
VMAT2
VGLUT2
% Syt2+ varicosities
Str.
Hipp.
PO
DLG
VPN
E
VMAT2
VGLUT2
Syt2 (a.u.)
Str.
Hipp.
PO
DLG
VPN

Figure 4. Expression of syt2 reveals heterogeneity among VGLUT2$^+$ glutamate neurons.

A. Example of 3D surfaces generated in a z-stack based on staining for syt2 (cyan, panel 1) or VGLUT2 (yellow, panel 2). Panel 3 shows syt2 and VGLUT2 surfaces in the same 3D section. In panel 4, syt2-positive VGLUT2 surfaces are shown in green and syt2-negative VGLUT2 surfaces are shown in red. A varicosity is considered syt2-positive if >40% of its volume overlaps with syt2 signal. Scale bar = 4 µm.

B. A single plane of a confocal image of a fixed brain slice from a HA-VMAT2 KI mouse acquired in the lateral geniculate nucleus (DLG). The slice is stained for HA-VMAT2, syt2 and VGLUT2. White arrowheads point to VMAT2 and orange arrowheads to a VGLUT2 varicosities. Scale bar = 3 µm.

C. Magnified view of the area highlighted by white box in B and plot profile of fluorescence intensities in three channels along the line ROI.

D. Percentage of VGLUT2 and HA-VMAT2 varicosities that contain syt2 signal in different brain regions. Each data point represents the percentage of syt2-positive varicosities per z-stack. Data indicate mean ± SEM. * = 0.0175, *** < 0.001, **** < 0.0001 by two-tailed unpaired t-test.

E. Quantification of mean syt2 intensity in HA-VMAT2 and VGLUT2 surfaces across brain regions. Each data point represents an analyzed z-stack. Data indicate mean ± SEM. * = 0.0105, ** = 0.0047 by two-tailed unpaired t-test.

Str. – striatum, Hipp. – CA2 region of the hippocampus, PO – posterior complex, VPN – ventral posteromedial nucleus.

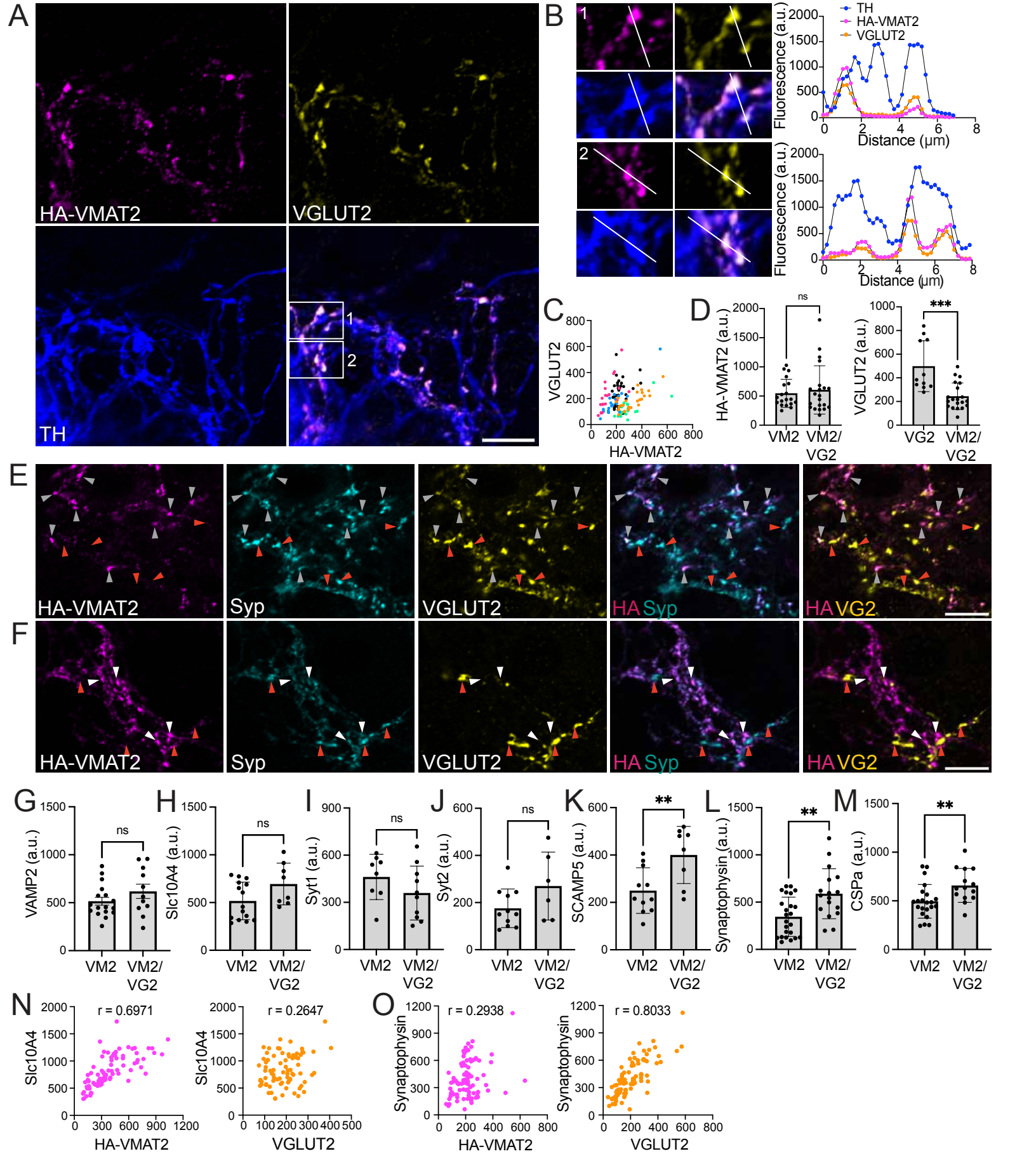
A
HA-VMAT2
VGLUT2
TH
1
2
B
TH
HA-VMAT2
VGLUT2
Fluorescence (a.u.)
Distance (μm)
C
VGLUT2
HA-VMAT2
D
HA-VMAT2 (a.u.)
VGLUT2 (a.u.)
ns
***
VM2
VM2/VG2
VG2
E
HA-VMAT2
Syp
VGLUT2
HA Syp
HA VG2
F
G
VAMP2 (a.u.)
H
Slc10A4 (a.u.)
I
Syt1 (a.u.)
J
Syt2 (a.u.)
K
SCAMP5 (a.u.)
L
Synaptophysin (a.u.)
M
CSPa (a.u.)
**
N
r = 0.6971
r = 0.2647
Slc10A4
O
r = 0.2938
r = 0.8033
Synaptophysin

Figure 5. SV protein composition of VMAT2-only versus VMAT2$^+$/VGLUT2$^+$ release sites.

A. Confocal image of a VGLUT2-positive DA neuron in a primary midbrain culture from HA-VMAT2 KI mice. Scale bar = 10 µm.

B. Magnified view of areas indicated by white boxes in A and plot profile of HA-VMAT2, VGLUT2 and TH signal along the line ROI showing overlapping VGLUT2 and HA-VMAT2 peaks in a DA neuron.

C. Scatter plot of HA-VMAT2 and VGLUT2 signal in individual presynaptic varicosities from one data set. Each color represents varicosities from one image (likely corresponding to a single cell).

D. Quantification of HA-VMAT2 signal in the presynaptic terminals of dopamine-only versus VMAT2$^+$/VGLUT2$^+$ neurons and VGLUT2 signal in glutamate-only versus VMAT2$^+$/VGLUT2$^+$ neurons. Each data point represents mean of individual ROIs per image. Data indicate mean ± SEM. *** = 0.0006 by Mann-Whitney test.

E. Confocal image of a coreleasing neuron and adjacent glutamate-only terminals stained for TH (not shown), synaptophysin, HA-VMAT2 and VGLUT2. Gray arrowheads point to VGLUT2$^+$/VMAT2$^+$ varicosities and orange arrowheads to VGLUT2-only terminals. Note that all HA-VMAT2 varicosities have detectable VGLUT2 signal. Scale bar = 10 µm.

F. Confocal image of a dopamine-only neuron and an adjacent glutamate-only neuron stained for TH (not shown), synaptophysin, HA-VMAT2 and VGLUT2. White arrowheads point to VMAT2 terminals and orange arrowheads to VGLUT2 terminals. Scale bar = 10 µm.

G-M. Quantification of VAMP2 (G), Slc10A4 (H), syt1 (I), syt2 (J), SCAMP5 (K), synaptophysin (L) and CSPα (M) in presynaptic terminals of dopamine-only or VMAT2$^+$/VGLUT2$^+$ neurons. Data indicate mean ± SEM. Each data point represents mean intensity of the signal for a protein of interest in all presynaptic varicosities per image. Data indicate mean ± SEM. ** <0.01 by unpaired t-test (K, M) or Mann-Whitney test (L).

N. Scatterplots showing correlation between Slc10A4 and HA-VMAT2 (magenta) or Slc10A4 and VGLUT2 (orange) signal in the same set of presynaptic terminals that contain both VGLUT2 and VMAT2.

O. Scatterplots showing correlation between synaptophysin and HA-VMAT2 (magenta) or synaptophysin and VGLUT2 (orange) signal in the same set of presynaptic terminals that contain both VGLUT2 and VMAT2.

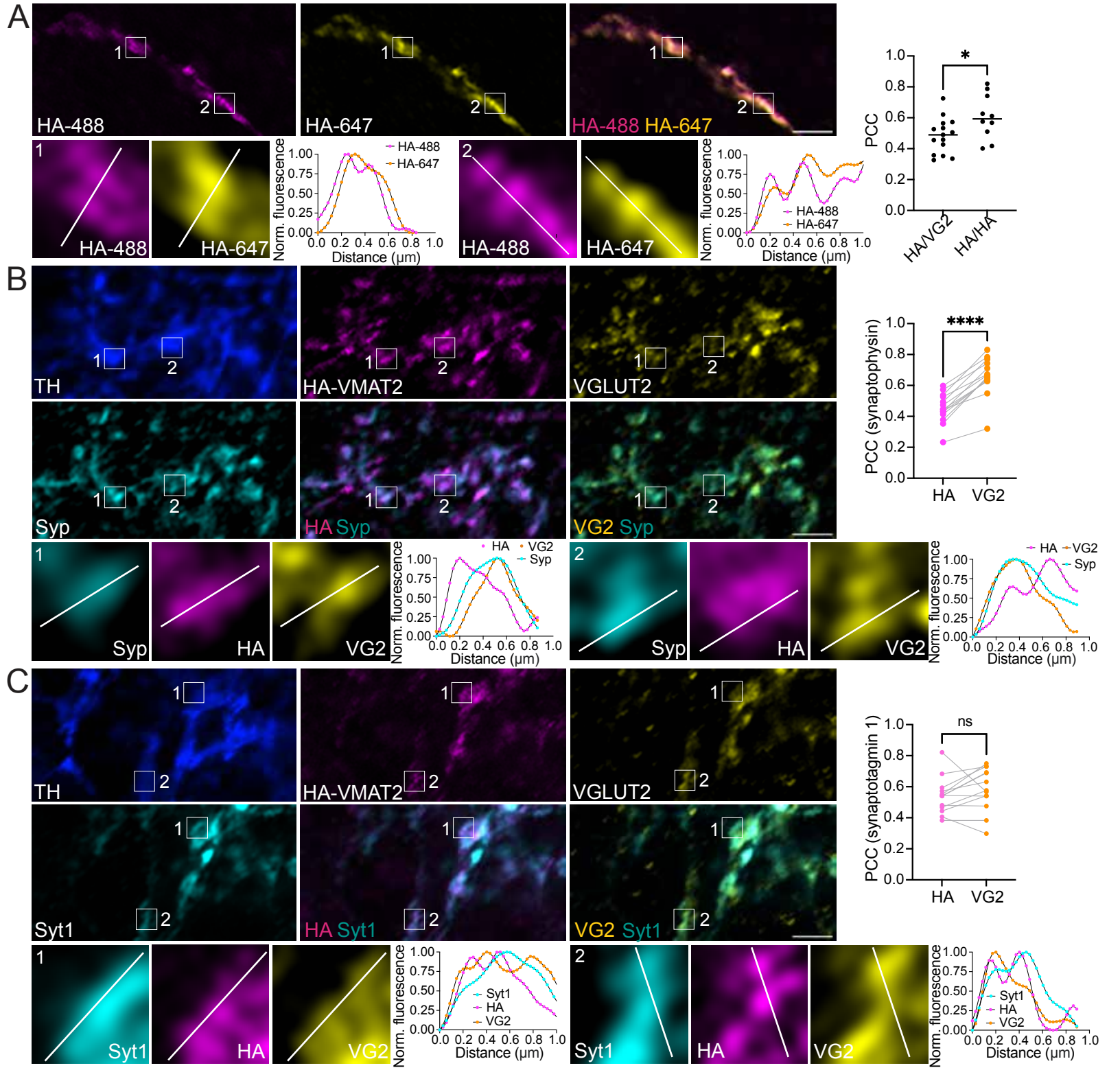
A
HA-488
HA-647
HA-488 HA-647
Norm. fluorescence
Distance (µm)
PCC
HA/VG2
HA/HA
B
TH
HA-VMAT2
VGLUT2
Syp
HA Syp
VG2 Syp
PCC (synaptophysin)
HA
VG2
C
Syt1
HA Syt1
VG2 Syt1
PCC (synaptotagmin 1)
ns

Figure 6. Synaptophysin is co-enriched with VGLUT2 signal in dopamine neuron presynaptic varicosities that contain both VMAT2 and VGLUT2.

A. A DA neuron from an HA-VMAT2 culture double stained for HA-VMAT2 using secondary antibodies coupled with Alexa 488 and Alexa 647 fluorophores. Scale bar = 2 µm.

Quantification shows Pearson's correlation coefficient (PCC) in individual varicosities for HA imaged in two channels versus for HA and VGLUT2 measured in data sets shown in B and C. Data indicate mean ± SEM. Each data point represents the mean of individual varicosities per image. * = 0.0265 by unpaired t-test. N = 10 HA/HA and 15 HA/VGLUT2 coverslips from two independent cultures.

Insets show magnification of areas indicated with white boxes with line ROIs and fluorescence profiles in HA-488 and HA-647 channels.

B. A VGLUT2-positive DA neuron from an HA-VMAT2 midbrain culture stained for TH, HA, VGLUT2 and synaptophysin (syp). Scale bar = 2 µm.

Quantification shows Pearson's correlation coefficient (PCC) for HA and synaptophysin versus VGLUT2 and synaptophysin quantified in varicosities that contain all three proteins. Data indicate mean ± SEM. Each data point represents the mean of individual varicosities per image. **** < 0.0001 by paired t-test. N = 14 images from two independent cultures.

Insets show magnification of areas indicated with white boxes with line ROIs and fluorescence profiles in HA, VGLUT2 and synaptophysin channels.

C. A VGLUT2-positive DA neuron from an HA-VMAT2 midbrain culture stained for TH, HA, VGLUT2 and synaptotagmin1 (syt1). Scale bar = 2 µm.

Quantification shows Pearson's correlation coefficient (PCC) for HA and synaptotagmin1 versus VGLUT2 and synaptotagmin1 quantified in varicosities that contain all three proteins. Data indicate mean ± SEM. Each data point represents the mean of individual varicosities per image. P = 0.2181 by paired t-test. N = 13 images from two independent cultures.

Insets show magnification of areas indicated with white boxes with line ROIs and fluorescence profiles in HA, VGLUT2 and synaptotagmin1 channels.

Images in all panels were acquired using the NSPARC detector and deconvolved using Nikon's built-in algorithm.

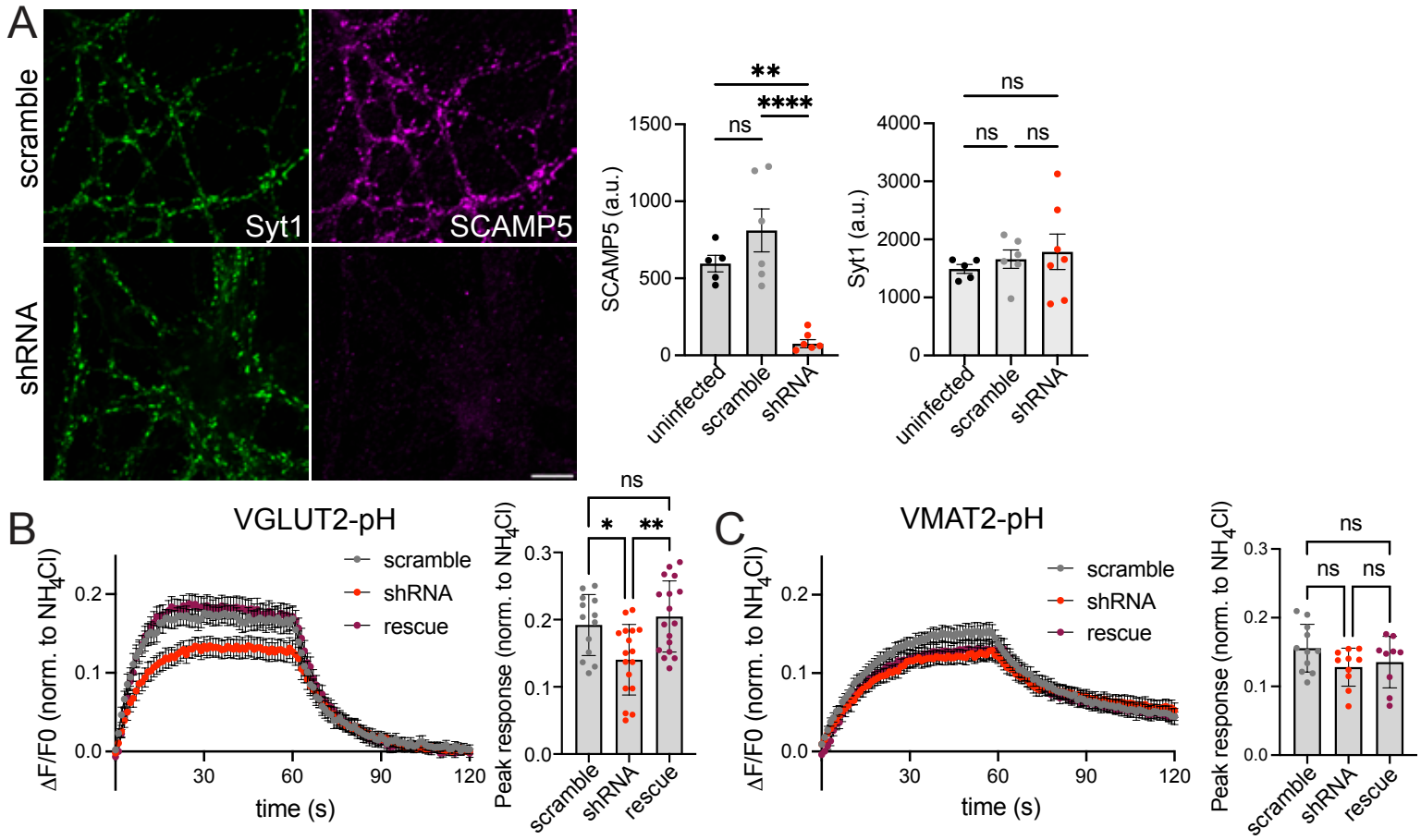
A
scramble
shRNA
Syt1
SCAMP5
SCAMP5 (a.u.)
Syt1 (a.u.)
ns
**
****
uninfected
scramble
shRNA
B
VGLUT2-pH
scramble
shRNA
rescue
ΔF/F0 (norm. to NH4Cl)
time (s)
Peak response (norm. to NH4Cl)
*
C
VMAT2-pH

Figure 7. Loss of SCAMP5 impairs synaptic recycling of VGLUT2 SVs without affecting VMAT2.

A. Confocal images and quantification of the fluorescence intensity of synaptotagmin1 and SCAMP5 in uninfected hippocampal neurons or cultures infected with shRNA targeting SCAMP5 or a scrambled control. Each data point represents mean presynaptic SCAMP5 or syt1 intensity per image. Data indicate mean ± SEM, ** $p = 0.0021$, **** $p < 0.0001$ by one-way ANOVA with Tukey's multiple comparisons. n = 5 uninfected, 6 scramble and 7 shRNA coverslips.

B-C. Average response curves and quantification of peak fluorescence intensity of VGLUT2-pHluorin (B) or VMAT2-pHluorin (C) to a 60s stimulation at 10 Hz. Data indicate mean ± SEM, * = 0.0225, ** = 0.017 by one-way ANOVA with Tukey's multiple comparisons. N = 13 scramble, 17 shRNA and 17 rescue coverslips for VGLUT2-pHluorin and 11 scramble, 10 shRNA and 9 rescue coverslips for VMAT2-pHluorin from three independent cultures.

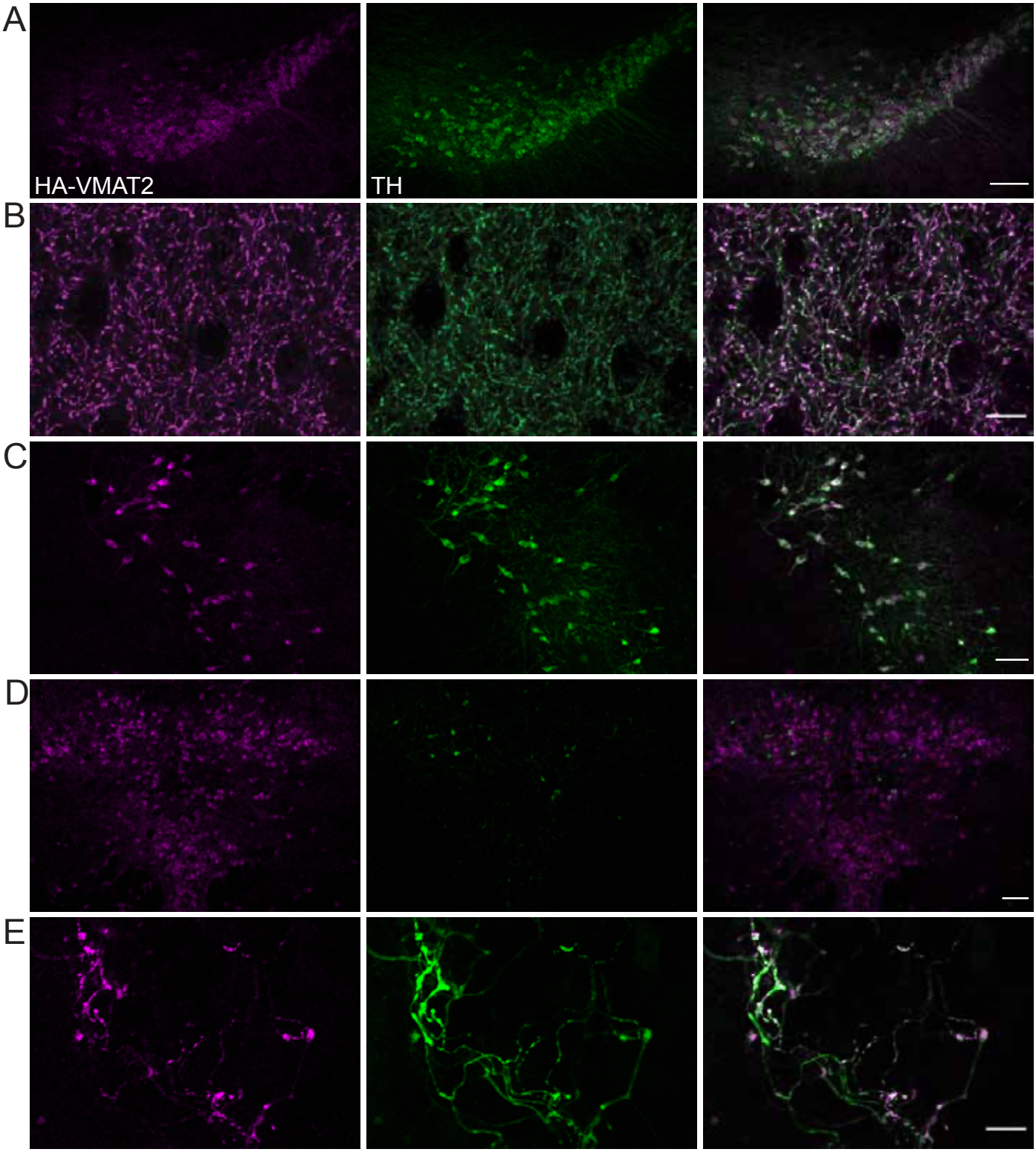
A
HA-VMAT2
TH
B
C
D
E

Supplementary figure 1. HA-VMAT2 is localized in cell bodies and neuronal processes of monoamine neurons.

A-D. Representative confocal images of HA-VMAT2 KI brain slices from the midbrain (A), striatum (B), locus coeruleus (C) and the raphe nucleus (D) stained for HA (magenta) and tyrosine hydroxylase (TH, green). Scale bar = 10 μm in all images.

E. Representative confocal image of a midbrain culture form HA-VMAT2 mice. Cultured neuron is stained for HA and TH. Scale bar = 10 μm.

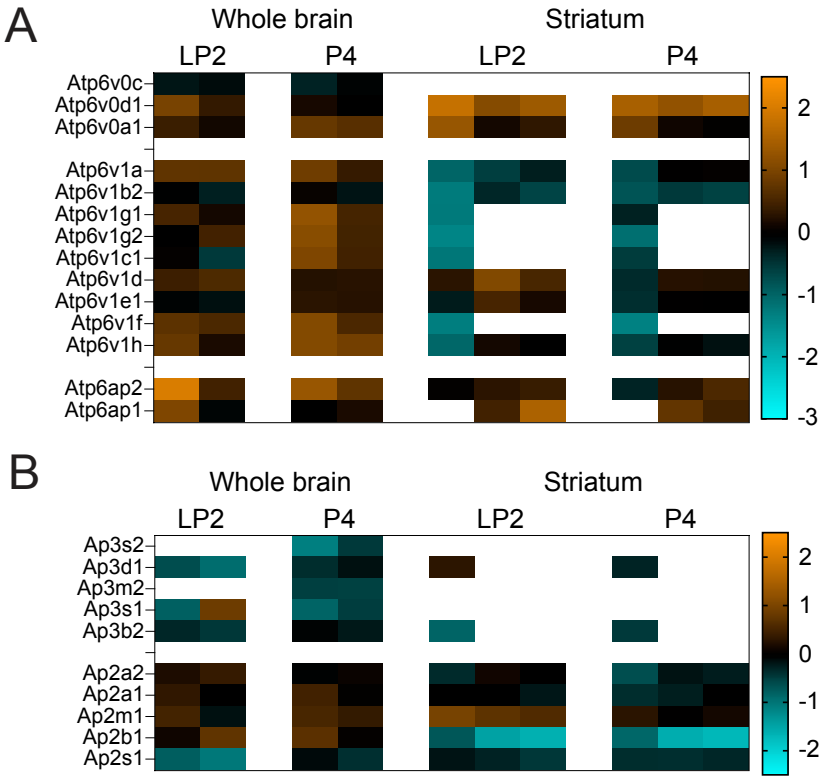
A
Whole brain
Striatum
LP2
P4
LP2
P4
Atp6v0c
Atp6v0d1
Atp6v0a1
Atp6v1a
Atp6v1b2
Atp6v1g1
Atp6v1g2
Atp6v1c1
Atp6v1d
Atp6v1e1
Atp6v1f
Atp6v1h
Atp6ap2
Atp6ap1
2
1
0
-1
-2
-3
B
Whole brain
Striatum
LP2
P4
LP2
P4
Ap3s2
Ap3d1
Ap3m2
Ap3s1
Ap3b2
Ap2a2
Ap2a1
Ap2m1
Ap2b1
Ap2s1
2
1
0
-1
-2

Supplementary figure 2. Abundance of V-ATPase, AP-2 and AP-3 subunits in VMAT2$^+$ and VGLUT2$^+$ SVs.

A. Subunits of the *v*-ATPase quantified on VMAT2 and VGLUT2 SVs isolated from whole brain or striatal samples from the HA-VMAT2 KI mouse. Data was normalized to the amount of total protein in each sample and is presented as a heat map of log2 values of VGLUT2/VMAT2 ratio. Each column represents an independent experiment.

B. Subunits of AP-2 and AP-3 quantified on VMAT2 and VGLUT2 SVs isolated from whole brain or striatal samples from the HA-VMAT2 KI mouse. Data was normalized to the amount of total protein in each sample and is presented as a heat map of log2 values of VGLUT2/VMAT2 ratio. Each column represents an independent experiment.

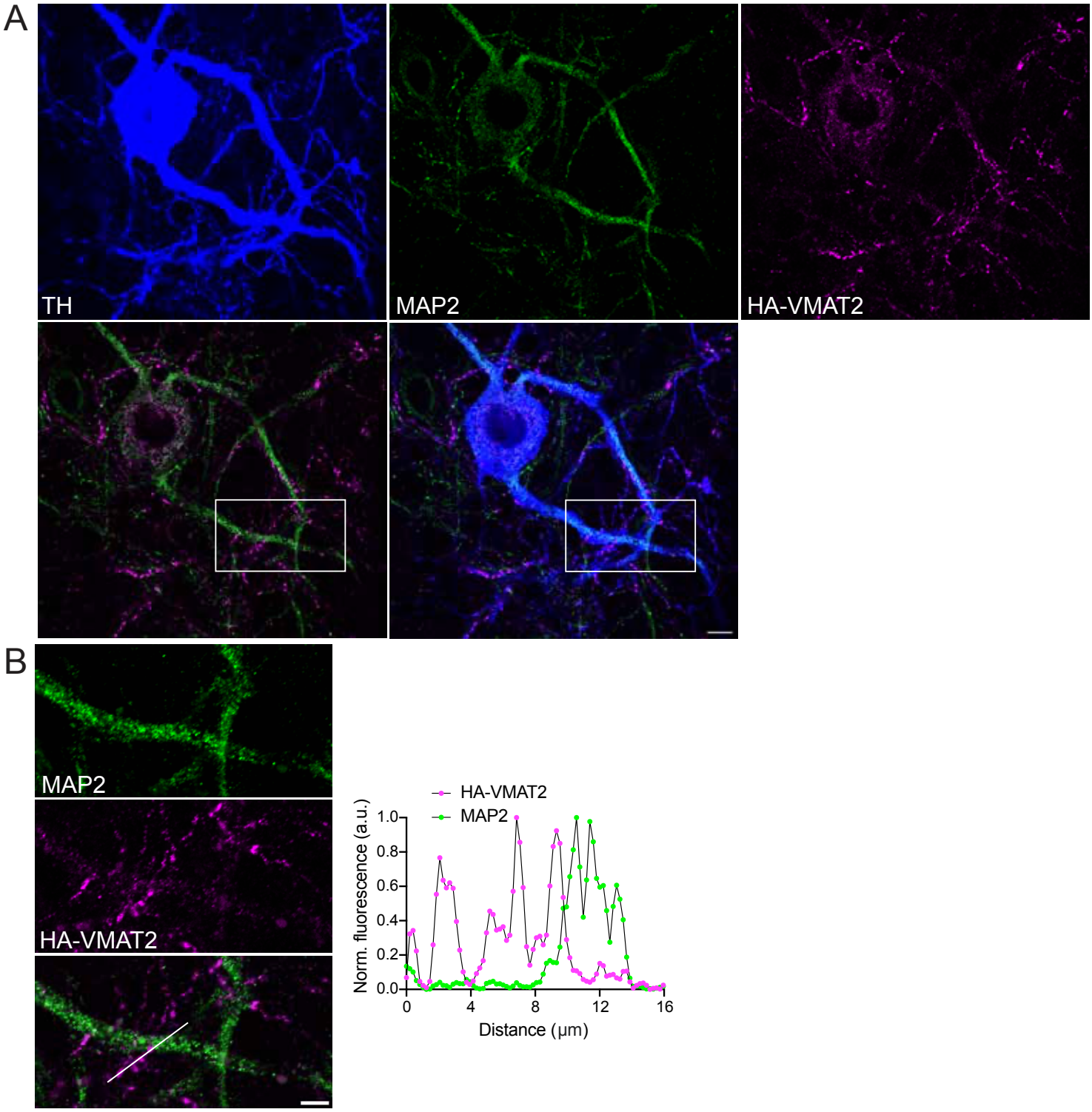
A
TH
MAP2
HA-VMAT2
B
MAP2
HA-VMAT2
HA-VMAT2
MAP2
Norm. fluorescence (a.u.)
1.0
0.8
0.6
0.4
0.2
0.0
0
4
8
12
16
Distance (µm)

Supplementary figure 3. HA-VMAT2 varicosities represent axonal vesicle clusters.

A. Confocal image of a dopamine neuron in a HA-VMAT2 KI midbrain culture stained for TH, somatodendritic protein MAP2 and HA-VMAT2. Scale bar = 10 μm.

B. Magnified view of the area highlighted by white box in A. Scale bar = 5 μm. Graph shows normalized fluorescence profiles of HA-VMAT2 and MAP2 along the line ROI shown in the merged image.

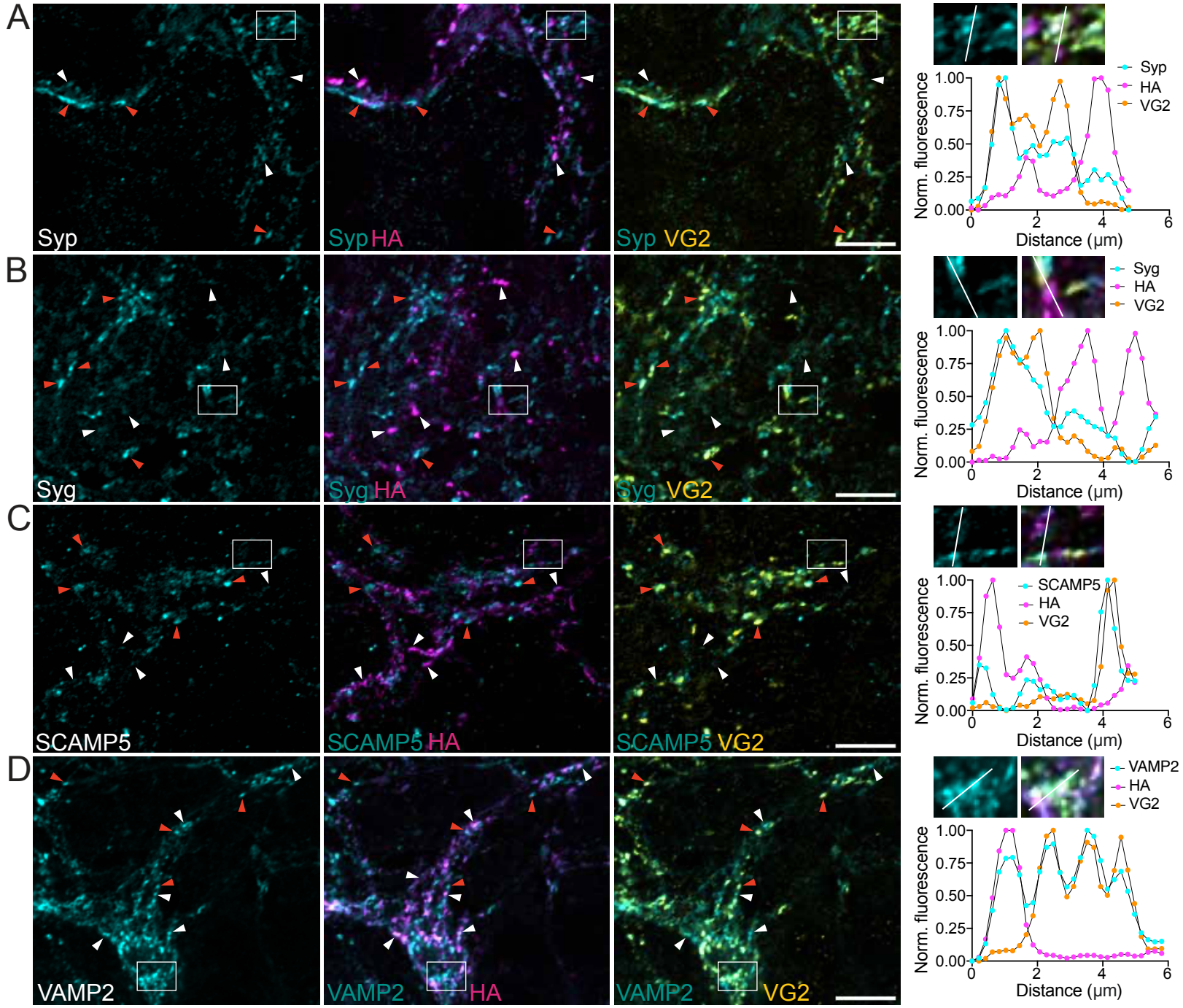
A
Syp
Syp HA
Syp VG2
Syp
HA
VG2
Norm. fluorescence
Distance (µm)
B
Syg
Syg HA
Syg VG2
Syg
HA
VG2
Norm. fluorescence
Distance (µm)
C
SCAMP5
SCAMP5 HA
SCAMP5 VG2
SCAMP5
HA
VG2
Norm. fluorescence
Distance (µm)
D
VAMP2
VAMP2 HA
VAMP2 VG2
VAMP2
HA
VG2
Norm. fluorescence
Distance (µm)

Supplementary figure 4. Presynaptic composition of dopamine and glutamate release sites in primary midbrain cultures.

A-D. Confocal images of midbrain cultures from HA-VMAT2 KI mice stained for HA-VMAT2, VGLUT2 and synaptophysin (A), synaptogyrin1 (B), SCAMP5 (C) or VAMP2 (D). White arrowheads point to HA-VMAT2 and orange arrowheads to VGLUT2 varicosities. Scale bars = 10 µm. Insets show magnification of the area indicated by the white boxes in larger images and a line ROI with corresponding fluorescence profiles in three channels shown below.

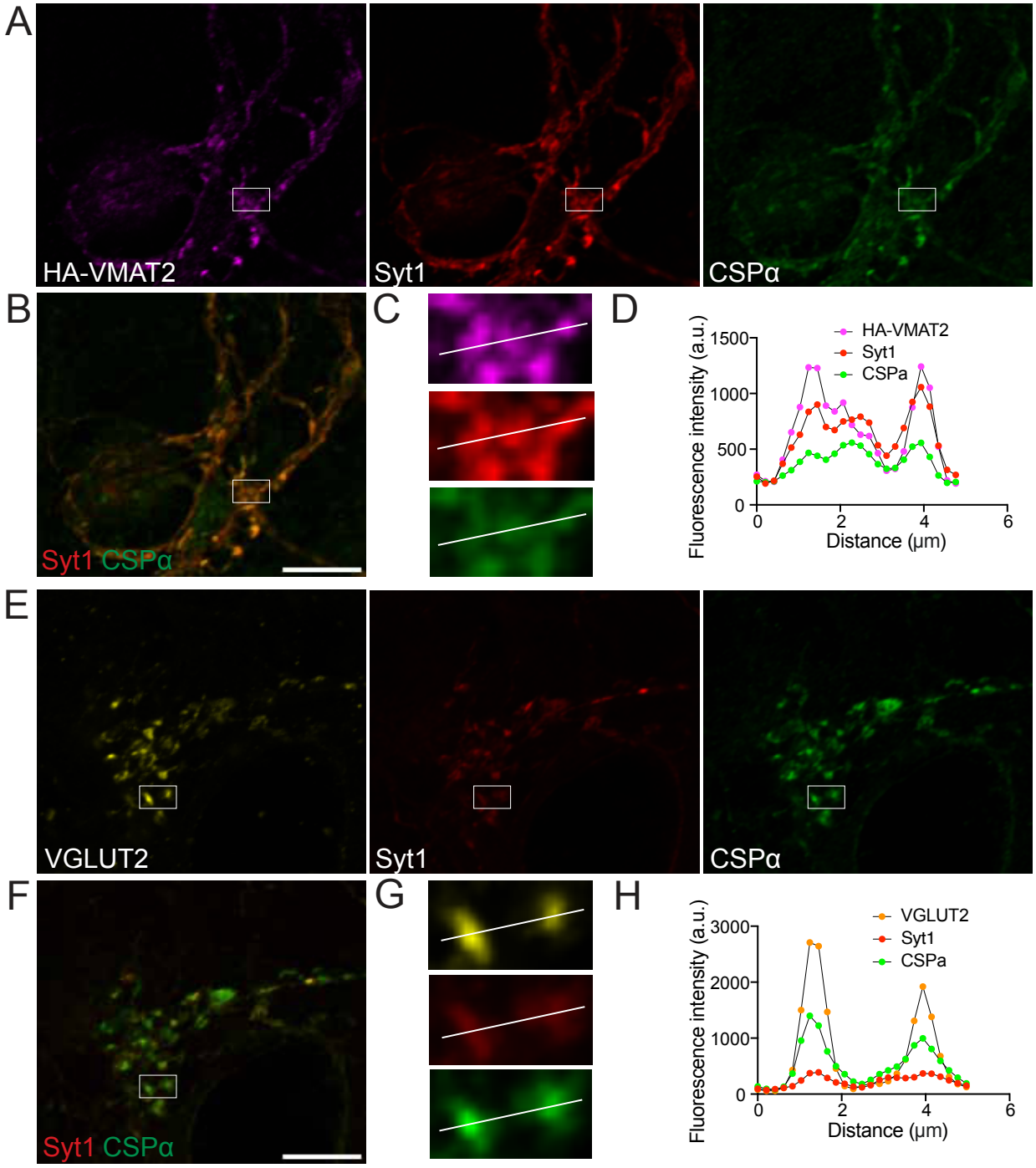
A
HA-VMAT2
Syt1
CSPα
B
Syt1 CSPα
C
D
HA-VMAT2
Syt1
CSPa
Fluorescence intensity (a.u.)
1500
1000
500
0
0
2
4
6
Distance (μm)
E
VGLUT2
Syt1
CSPα
F
Syt1 CSPα
G
H
VGLUT2
Syt1
CSPa
Fluorescence intensity (a.u.)
3000
2000
1000
0
0
2
4
6
Distance (μm)

Supplementary figure 5. VMAT2 and VGLUT2 varicosities differ in syt1/CSPα ratio.

A-D. A. Confocal image of a midbrain culture from HA-VMAT2 KI mice stained for HA-VMAT2, synaptotagmin1 and CSPα. B. Merge of synaptotagmin1 and CSPα channels. Scale bar = 10 µm. C. Magnified view of the area indicated by white box in A and B. D. Fluorescence profiles of HA-VMAT2, synaptotagmin1 and CSPα along the line ROI shown in C.

E-H. E. Confocal image of a midbrain culture from HA-VMAT2 KI mice stained for VGLUT2, synaptotagmin1 and CSPα. F. Merge of synaptotagmin1 and CSPα channels. Scale bar = 10 µm. G. Magnified view of the area indicated by white box in E and F. H. Fluorescence profiles of VGLUT2, synaptotagmin1 and CSPα along the line ROI shown in G.

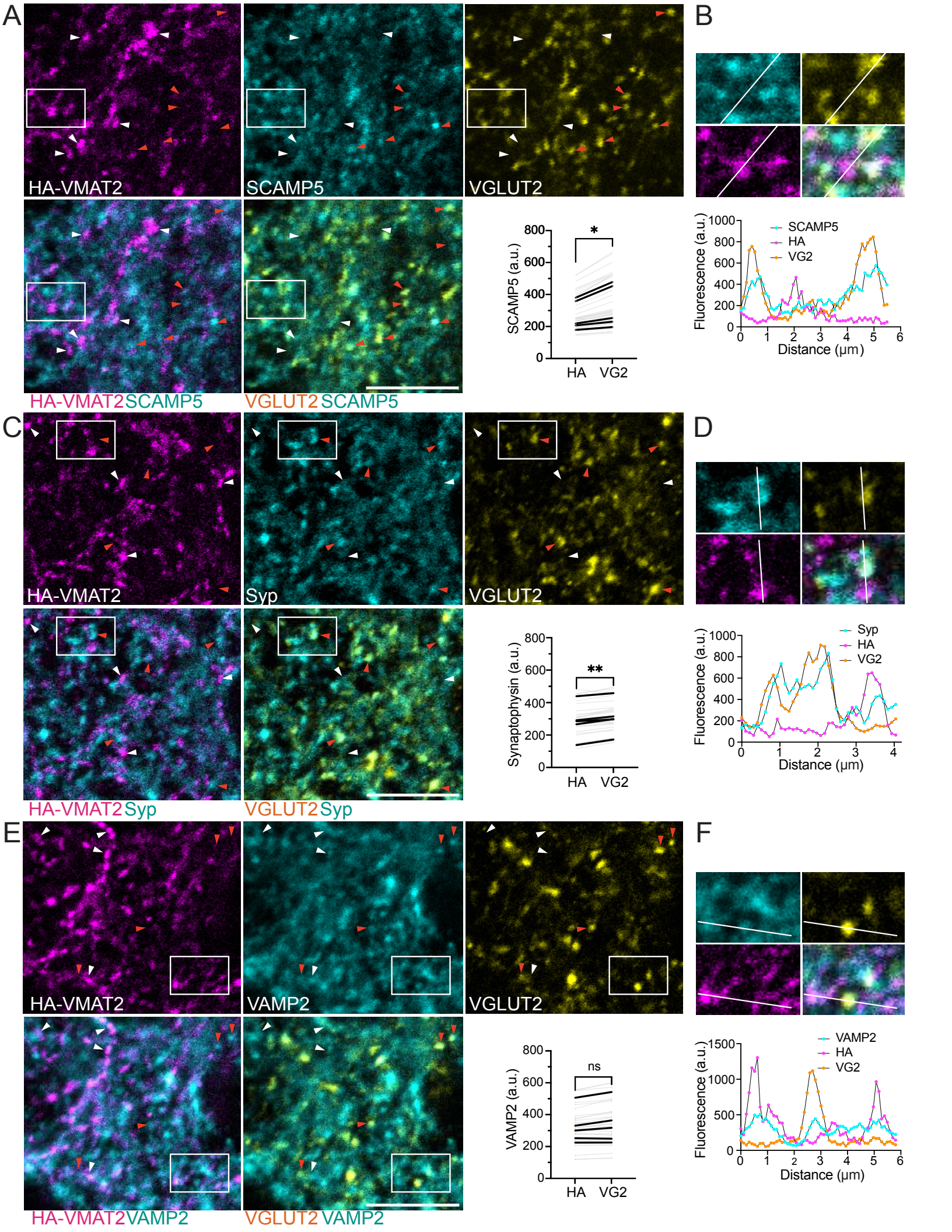
A
HA-VMAT2
SCAMP5
VGLUT2
HA-VMAT2 SCAMP5
VGLUT2 SCAMP5
SCAMP5 (a.u.)
800
600
400
200
0
*
HA
VG2
B
Fluorescence (a.u.)
1000
800
600
400
200
0
SCAMP5
HA
VG2
0 1 2 3 4 5 6
Distance (µm)
C
HA-VMAT2
Syp
VGLUT2
HA-VMAT2 Syp
VGLUT2 Syp
Synaptophysin (a.u.)
800
600
400
200
0
**
HA
VG2
D
Fluorescence (a.u.)
1000
800
600
400
200
0
Syp
HA
VG2
0 1 2 3 4
Distance (µm)
E
HA-VMAT2
VAMP2
VGLUT2
HA-VMAT2 VAMP2
VGLUT2 VAMP2
VAMP2 (a.u.)
800
600
400
200
0
ns
HA
VG2
F
Fluorescence (a.u.)
1500
1000
500
0
VAMP2
HA
VG2
0 1 2 3 4 5 6
Distance (µm)

Supplementary figure 6. Protein composition of VMAT2 and VGLUT2 varicosities in the striatum.

A-B. A. Confocal image of a single plane in a striatal slice from a HA-VMAT2 KI mouse stained for HA-VMAT2, SCAMP5 and VGLUT2 together with quantification of mean SCAMP5 intensity in 3D surfaces generated based on HA-VMAT2 or VGLUT2 signal. Gray lines show mean values of varicosities per image, black lines indicate the mean values per mouse. * = 0.0378 by paired t-test on mouse averages. Scale bar = 10 µm. White arrowheads point to HA-VMAT2 and orange arrowheads to a VGLUT2 varicosities. B. Magnified view of the area highlighted by white box in A and plot profile of fluorescence intensities in three channels along the line ROI.

C-D. C. Confocal image of a single plane in a striatal slice from a HA-VMAT2 KI mouse stained for HA-VMAT2, synaptophysin and VGLUT2 together with quantification of mean synaptophysin intensity in 3D surfaces generated based on HA-VMAT2 or VGLUT2 signal. Gray lines show mean values of varicosities per image, black lines indicate the mean values per mouse. ** = 0.0043 by paired t-test on mouse averages. Scale bar = 10 µm. White arrowheads point to HA-VMAT2 and orange arrowheads to a VGLUT2 varicosities. D. Magnified view of the area highlighted by white box in C and plot profile of fluorescence intensities in three channels along the line ROI.

E-F. E. Confocal image of a single plane in a striatal slice from a HA-VMAT2 KI mouse stained for HA-VMAT2, VAMP2 and VGLUT2 together with quantification of mean VAMP2 intensity in 3D surfaces generated based on HA-VMAT2 or VGLUT2 signal. Gray lines show mean values of varicosities per image, black lines indicate the mean values per mouse. P = 0.1129 by paired t-test on mouse averages. Scale bar = 10 µm. White arrowheads point to HA-VMAT2 and orange arrowheads to a VGLUT2 varicosities. F. Magnified view of the area highlighted by white box in E and plot profile of fluorescence intensities in three channels along the line ROI.

METHODS

Mice

Both male and female mice were used for all experiments. All mice received unlimited food and water and were exposed to 12h/12h light/dark cycle. HA-VMAT2 KI transgenic mice were used for proteomics, primary dopamine neuron cultures and tissue staining. C57BL6J mice were used for primary hippocampal cultures. All experiments with animals were performed according to the National Institutes of Health Guide for Care and Use of Laboratory Animals and were approved by the Cedars-Sinai Medical Center Institutional Animal Care and Use Committee.

Generation of HA-VMAT2 knock-in mice

To generate the HA-VMAT2 knock-in mouse model, we used the CRISPR/Cas9 genome editing system. A guide RNA was designed to target the N-terminal tail of mouse VMAT2 (target sequence 5'-CAGCAGCACCAGATCGCTCA-3'). An ssDNA donor template was constructed to contain the sequence of the hemagglutinin tag followed by a linker consisting of two glycines and a modified PAM sequence. The donor sequence was flanked by 60 bp homology arms on both sides. Cas9 together with the gRNA and ssDNA donor were co-injected into C57BL/6 mouse embryos at a single cell stage at the University of California, San Francisco Transgenic Gene Targeting Core.

Molecular biology

SCAMP5-specific small hairpin RNA (shRNA) was designed with the aid of the InvivoGen siRNA Wizard Online Tool to target the mouse SCAMP5 cDNA sequence. SCAMP5 knock-down (TGCTCTTAGCATGGTTCATAA) and a scrambled control sequences were inserted into the pLKO.1 lentiviral vector[102] obtained from Addgene using AgeI and EcoRI restriction sites. An shRNA-resistant SCAMP5 rescue sequence was designed with the help of the Java Codon Optimization Tool, effectively creating silent mutations in the target region sequence which would be unrecognizable by the shRNA but would still code for SCAMP5. A custom lentiviral vector was ordered through Vector Builder and includes the human synapsin promoter, SCAMP5 rescue sequence, and mCherry to mark infected cells.

Lentivirus production

Low-passage LentiX HEK cells (Takara, cat. # 632180) were seeded onto 6-well plates and transfected the following day with 1.5 µg of third-generation lentiviral vector FUGW encoding the

gene of interest together with 0.5 µg each of packaging plasmids pRRE, pVSVG and pRSV-Rev using the FuGene HD transfection reagent (Promega, cat. # E2311) according to manufacturer's instructions. Next morning, culture medium was changed into fresh Neurobasal. Viral supernatant was collected 47 hours after transfection and concentrated 10x using Lenti-X Concentrator (Takara, cat. # 631231). Aliquots were stored at -80C until use.

Primary neuron culture

Hippocampal neurons: Hippocampi were dissected from P0 mice of both sexes in Hank's Balanced Salt Solution (HBSS) containing 10 mM HEPES and 20 mM glucose, dissociated in 0.25% trypsin, washed three times with Minimal Essential Medium containing 1x B27 (GIBCO, 17504-044), 2 mM glutamax (GIBCO, 35050-061), 5% FBS (HyClone, defined), 21 mM glucose (Sigma, G8769) and 1x penicillin/streptomycin (Corning, 30-002-CL), triturated and plated on poly-L-lysine coated coverslips at 350 cells/mm2 in the above Minimal Essential Media. After one day *in vitro* (DIV1), 3/4 of the medium was changed to Neurobasal (GIBCO, 21103-049) with B27, glutamax and penicillin/streptomycin. Cells were infected with lentiviruses encoding VGLUT2-pHluorin, VMAT2-pHluorin, and/or shRNA SCAMP5 KD, scramble or rescue on DIV 4-5. 4 µM cytosine arabinoside was added on DIV7 to inhibit glial proliferation.

Dopamine neurons: Ventral midbrain regions containing substantia nigra and ventral tegmental area were dissected from neonatal HA-VMAT2 KI mice of both sexes. Tissue pieces were dissected in Hank's Balanced Salt Solution (HBSS) containing 10 mM HEPES and 20 mM glucose, dissociated in papain (Worthington) for 15 minutes, washed with media containing 60% Neurobasal-A, 30% Basal Media Eagle, 10% fetal bovine serum (HyClone, defined), 1x B27, 2 mM GlutaMAX, 10 ng/mL glial cell line-derived neurotrophic factor (Millipore, MA, USA) and 1x penicillin/streptomycin, triturated and plated in the above media at 1500 cells/mm^2.

Synaptic Vesicle Preparation

Whole brains or striatal tissue from 10-15 HA-VMAT2 KI mice was pooled per replicate. Tissue was homogenized by 9 strokes at 900 rpm in cold homogenization buffer (0.3M sucrose, 1mM Mg-EGTA, 10 mM HEPES-Tris, pH 7.4) with cOmplete protease inhibitors (Roche, cat. # 11836170001) using a glass teflon homogenizer. The homogenate (H) was centrifuged at 871 g for 10 min at 4 °C in an SS34 rotor (Sorvall). Pellet was discarded and supernatant (S1) was sedimented at 12,000 g for 15 min at 4 °C in an SS34 rotor. Both pellet P2 and supernatant S2 were collected and processed in parallel.

Pellet (P2) that is enriched in synaptosomes was resuspended in 10 mL homogenization buffer. Resuspended P2 was sedimented at 14,500 g for 15 min at 4 °C in an SS34 rotor, the supernatant (S2′) was removed and pooled with S2. P2′ was resuspended in 1.2 mL homogenization buffer and then subjected to osmotic lysis for 45 min in 13.5 ml cold water with 8 mM HEPES-Tris, pH 7.4. The lysed P2′ was homogenized using five strokes at 3,000 rpm and centrifuged at 32,500 g for 20 min. The lysed supernatant (LS1) was transferred into a new ultracentrifuge tube and centrifuged at 280,000 g for 2 h using a Beckman 70 Ti rotor. Supernatant was discarded and pellet (LP2) was resuspended in salt buffer (150 mM NaCl, 1 mM Mg-EGTA, 10 mM HEPES, pH 7.4) by repeated pipetting.

The S2/S2' samples were homogenized by 5 strokes at 3000 rpm and sedimented 32,500 g for 20 min. The resulting supernatant S3 was transferred to a new ultracentrifuge tube and centrifuged at 280,000 g for 2 h using a Beckman 70 Ti rotor. Supernatant S4 was discarded and pellet P4 was collected and resuspended in salt buffer like LP2 described above.

To obtain pure SVs, LP2 and P4 fractions were further purified by velocity sedimentation through a continuous 5–25% glycerol gradient at 270,000 g for 1 h and 4 min in a Beckman SW 41 rotor. 0.5 mL fractions were collected from top to bottom. Fractions 7-12 were pooled and dialyzed over night at 4C in 150 mM NaCl, 1 mM Mg-EGTA, 10 mM HEPES, pH 7.4.

Immunoisolation

Dialyzed synaptic vesicles were supplemented with 1% lysine and 1% glycine to reduce non-specific binding and cOmplete protease inhibitors (Roche, cat. # 11836170001). Vesicles were incubated on the rotator with anti-HA (Cell Signaling, Cat # 3724 for whole brain samples and Covance, AB_291262 for striatal samples), anti-VGLUT2 (Synaptic Systems, cat. # 95E11) antibodies for 2 hours at 4C. 5 µL of antibody was added per 2 mL of vesicle suspension.

In parallel, equal volumes of Dynabeads with protein A (Invitrogen 10001D) and protein G (Invitrogen 10003D) were washed three times in salt buffer with protease inhibitors and lysine/glycine. 50 µL of protein A/G beads was then added to 2 mL of synaptic vesicle/antibody mix and incubated on the rotator for 1 hour at 4C. Beads were washed three times in salt buffer and stored at -80C until processing for mass spectrometry.

Mass Spectrometry

Peptide and protein identification and TMT quantitation: Peak lists were generated using the PAVA in-house software[103]. All generated peak lists were searched against the mouse subset of the SwissProt database (SwissProt.2019.07.31, 17,026 entries searched) using Protein

Prospector[104] with the following parameters: Enzyme specificity was set as Trypsin, and up to 2 missed cleavages per peptide were allowed. Carbamidomethylation of cysteine residues, and TMTPro16plex labeling of lysine residues and N-terminus of the protein were allowed as fixed modifications. N-acetylation of the N-terminus of the protein, loss of protein N-terminal methionine, pyroglutamate formation from of peptide N-terminal glutamines, and oxidation of methionine were allowed as variable modifications Mass tolerance was 5 ppm in MS and 30 ppm in MS/MS. The false discovery rate was estimated by searching the data using a concatenated database which contains the original SwissProt database, as well as a version of each original entry where the sequence has been randomized. A 1% FDR was permitted at the protein and peptide level.

For quantitation, only unique peptides were considered. Relative quantization of peptide abundance was performed by calculating the intensity of reporter ions corresponding to the different TMT labels present in MS/MS spectra. Intensities were determined by Protein Prospector. Median intensities of the reporter ions for all peptide spectral matches (PSMs) on each TMT channel were used to normalize individual (sample-specific) intensity values. In addition to classical SV proteins, we detected peptides associated with frequent contaminants of SV preparations (proteasomes, ribosomes). To improve detection of differences in SV proteins, contaminants associated with other organelles were excluded from analysis. For each PSM, relative abundances were calculated as ratios of signal in VGLUT2 versus matching VMAT2 samples. For relative amounts of total protein, peptide ratios were aggregated to the protein levels using median values of the log 2 ratios. Statistical significance was determined comparing the log2 ratios to a log2 reference value of 0 using a two-tailed t-test.

Western blot

Proteins were separated by electrophoresis on 4-20% precast polyacrylamide gels (Bio-Rad) and transferred to nitrocellulose membranes. Membranes were blocked in 5% milk tris buffered saline with 0.1% Tween. Primary antibodies were incubated overnight at 4C and IRDye 680- or IRDye 800-coupled secondary antibodies (Rockland Immunochemicals) for 1 hour at room temperature.

Immunohistochemistry

To obtain fixed brain, mice were perfused with cold PBS, followed by 4% PFA in PBS. Brains were postfixed overnight in 4% PFA and cryoprotected in PBS containing 30% sucrose. 35 µm sections were cut using a Leica CM3050 S cryostat and floating sections were stored in PBS with 0.02% Na-azide. Cultured cells were fixed for 15 minutes in 4% PFA in PBS and washed three

times in PBS. Floating sections as well as cultured cells were blocked and permeabilized in PBS containing 5% normal goat serum and 0.2% Triton X-100. Primary and secondary antibodies were diluted in PBS containing 2.5% normal goat serum and 0.2% Triton X-100 in PBS for staining slices and in 2.5% normal goat serum in PBS for staining cultured cells. Primary antibodies were incubated overnight at 4°C for tissue sections and 2 hours at room temperature for cultured cells. Secondary antibodies were incubated with tissue sections for 2 hours and cultured cells for 1 hour in the dark at room temperature. Slices were mounted in Fluoromount-G (SouthernBiotech) or Vectashield (Vector Laboratories). Antibodies were used at the following dilutions:

SYT1 Ms 1:5000 Synaptic Systems 105011
TH Ms 1:1000 EMD Millipore MAB5280
VG2 Gp 1:1000 Synaptic Systems 135404
VG2 Ch 1:1000 Synaptic Systems 135416
SYT2 Gp 1:1000 Synaptic Systems 105225
HA Rt 1:500 Roche 11867423001
SYPH Ms 1:500 Synaptic Systems 101011
SYPH Gp 1:100 Synaptic Systems 101 308
VAMP2 Rb 1:500 Synaptic Systems 104202
CSP Rb 1:500 Synaptic Systems 154003
SLC10a4 Rb 1:200 Sigma HPA028835
SYG Rb 1:100 Synaptic Systems 103002
SCAMP5 Rb 1:50 Invitrogen PA5-61269
All secondary antibodies were used at 1/750 dilution.

Imaging of fixed cultures and brain slices

Images of fixed cultured neurons and brain slices were acquired using the Nikon Eclipse Ti2-E Microscope equipped with AR or AX confocal, AR1-DUG2 scan head with gallium arsenide phosphide detector unit and a Plan Apo VC 60x DIC N2 oil objective. Lasers (405 nm, 488 nm, 561 nm and 640 nm) were used for excitation and ET525/50, ET593/46 and ET700/75 filters for emission. Colocalization within release sites of dopamine/glutamate coreleasing neurons was quantified on images acquired on a Nikon Eclipse Ti2-E microscope equipped with a AX confocal module and a NSPARC (Nikon Spatial Array Confocal) detector[60]. Lense alignment was re-calibrated every 45 minutes during imaging. Deconvolution was performed using Nikon's built-in deblurring algorithm.

Tissue Section 3D Analysis: Presynaptic protein abundance in brain slices was quantified using Imaris software (Oxford Instruments). Z stacks were acquired with a z-step of 0.125 µm and 3D surfaces were generated based on HA-VMAT2 and VGLUT2 signal. Thresholds for surfaces were selected manually and kept consistent within-mouse for all analyses. For Syt-2 colocalization analysis, surfaces were generated manually and kept consistent within-mouse except for images of the lateral geniculate nucleus, where the morphology of VGLUT2 presynapses departed considerably from all other regions and unique thresholds were used. Mean signal for the protein of interest was measured in HA-VMAT2 versus VGLUT2 surfaces and obtained values were compared within image, and a paired t-test was applied for both slice- and mouse-level statistics.

Image analysis in fixed cultures

Presynaptic protein abundance in midbrain cultures was quantified in imageJ. Regions of interest (ROI) were selected based on HA-VMAT2 or VGLUT2 signal or by the presence of both transporters. The fluorescence intensity of proteins of interest was measured in the three sets of ROIs. For colocalization analysis in dopamine/glutamate coreleasing neurons, images were processed using the Coloc2 plugin in imageJ.

Live imaging

Hippocampal cultures between 16-19 DIV were mounted in a laminar flow perfusion and stimulation chamber (Warner Instruments RC-21BRFS) on an inverted Nikon Eclipse Ti fluorescence microscope, Hamamatsu ORCA-Flash4.0 camera, and Nikon Plan Apo λD 60x oil objective. Fluorescence signals were collected under epifluorescence illumination using 465/95 nm excitation and 515/55 nm emission for pHluorin. Action potentials (APs) were evoked by passing 1 ms bipolar current pulses through platinum electrodes, to yield fields of 5–10 V/cm. Cells were continuously perfused with Tyrode's buffer (119 mM NaCl, 25 mM HEPES, 2 mM $CaCl_2$, 2 mM $MgCl_2$, 2.5 mM KCl, and 30 mM glucose at pH 7.4) containing 10 µM 6-cyano-7-nitroquinoxaline-2,3-dione (CNQX) and 10 µM 3-(2-carboxypiperazin-4-yl)propyl-1-phosphonic acid (APV). Total cellular pHluorin content was revealed by applying Tyrode's buffer with 50 mM NH_4Cl, where NaCl was reduced to 69 mM. Imaging was done at 37°C. For analysis, synaptic boutons were selected manually. Background fluorescence was subtracted and fluorescence intensity in the synaptic boutons was normalized to pre-stimulation baseline and to unquenched (total) pHluorin fluorescence in NH_4Cl.

Statistics

Statistical analysis was performed using GraphPad Prism 10 software. The Shapiro-Wilk test was used to assess the normal distribution of data. For comparing two conditions, two-tailed paired or unpaired t-test (indicated in text and figure legends) was used if data was normally distributed and Mann-Whitney test was used if data that did not pass the test for normality. One-way ANOVA with Tukey's post hoc test was used for comparing more than two samples. Data are presented as mean ± SEM and statistical significance as * $P < 0.05$, ** $P < 0.01$, *** $P < 0.001$, and **** $P < 0.0001$.

ACKNOWLEDGEMENTS

This work was supported by grants from the Brain and Behavior Research Foundation (29845) and The Larry L. Hillblom Foundation (2022-A-004-SUP) as well as start-up funds from the Cedars-Sinai Medical Center to K.S. R.H.E. is supported by R01NS103938 and R01NS129803 from the National Institute of Neurological Disorders and Stroke. We are grateful for imaging support from V. Krishnan Ramanujan and Mingtian Che from the Cedars-Sinai Biobank and Research Pathology Resource. Mass spectrometry was performed at the Mass Spectrometry Resource at UCSF, which is supported by the Dr. Miriam and Sheldon G. Adelson Medical Research Foundation (J.A.O.-P. & A.L.B.).

AUTHOR CONTRIBUTIONS

K.S. and R.H.E. designed research; H.A., A.J.D., H.X., J.A.O.-P., J.A., A.S., B.G., N.C. and K.S. performed experiments; H.A., A.J.D., H.X., J.A.O.-P., J.A., A.S., B.G. and K.S. analyzed data; A.L.B, R.H.E. and K.S. acquired funding; K.S. wrote the paper with feedback from H.A., A.J.D., H.X., J.A.O.-P., A.S. and R.H.E.

COMPETING INTERESTS

R.H.E. is a consultant for Nine Square Therapeutics. Other authors have no competing interests to declare.

REFERENCES

1. Takamori, S. *et al.* Molecular Anatomy of a Trafficking Organelle. *Cell* **127**, 831–846 (2006).

2. Südhof, T. C. & Rothman, J. E. Membrane Fusion: Grappling with SNARE and SM Proteins. *Science* **323**, 474–477 (2009).

3. Südhof, T. C. The Presynaptic Active Zone. *Neuron* **75**, 11–25 (2012).

4. Markram, H., Wang, Y. & Tsodyks, M. Differential signaling via the same axon of neocortical pyramidal neurons. *Proc National Acad Sci* **95**, 5323–5328 (1998).

5. Ding, J., Peterson, J. D. & Surmeier, D. J. Corticostriatal and thalamostriatal synapses have distinctive properties. *J Neurosci Official J Soc Neurosci* **28**, 6483–92 (2008).

6. Scanziani, M., Gähwiler, B. H. & Charpak, S. Target cell-specific modulation of transmitter release at terminals from a single axon. *Proc. Natl. Acad. Sci.* **95**, 12004–12009 (1998).

7. Dittman, J. S., Kreitzer, A. C. & Regehr, W. G. Interplay between Facilitation, Depression, and Residual Calcium at Three Presynaptic Terminals. *J. Neurosci.* **20**, 1374–1385 (2000).

8. Neher, E. Merits and Limitations of Vesicle Pool Models in View of Heterogeneous Populations of Synaptic Vesicles. *Neuron* **87**, 1131–1142 (2015).

9. Schikorski, T. & Stevens, C. F. Morphological correlates of functionally defined synaptic vesicle populations. *Nat. Neurosci.* **4**, 391–395 (2001).

10. Chamberland, S. & Tóth, K. Functionally heterogeneous synaptic vesicle pools support diverse synaptic signalling. *J. Physiol.* **594**, 825–835 (2016).

11. Atwood, H. L. & Karunanithi, S. Diversification of synaptic strength: presynaptic elements. *Nat. Rev. Neurosci.* **3**, 497–516 (2002).

12. Asmerian, H., Alberts, J., Sanetra, A. M., Diaz, A. J. & Silm, K. Role of adaptor protein complexes in generating functionally distinct synaptic vesicle pools. *J. Physiol.* (2024) doi:10.1113/jp286179.

13. Saunders, A. *et al.* Molecular Diversity and Specializations among the Cells of the Adult Mouse Brain. *Cell* **174**, 1015-1030.e16 (2018).

14. Yao, Z. *et al.* A high-resolution transcriptomic and spatial atlas of cell types in the whole mouse brain. *Nature* **624**, 317–332 (2023).

15. Siletti, K. *et al.* Transcriptomic diversity of cell types across the adult human brain. *Science* **382**, eadd7046 (2023).

16. Oostrum, M. van *et al.* The proteomic landscape of synaptic diversity across brain regions and cell types. *Cell* (2023) doi:10.1016/j.cell.2023.09.028.

17. Branco, T. & Staras, K. The probability of neurotransmitter release: variability and feedback control at single synapses. *Nat. Rev. Neurosci.* **10**, 373–383 (2009).

18. Descarries, L. & Mechawar, N. Ultrastructural evidence for diffuse transmission by monoamine and acetylcholine neurons of the central nervous system. *Prog Brain Res* **125**, 27–47 (2000).

19. Beaulieu, J.-M. & Gainetdinov, R. R. The Physiology, Signaling, and Pharmacology of Dopamine Receptors. *Pharmacol. Rev.* **63**, 182–217 (2011).

20. Schultz, W., Dayan, P. & Montague, P. R. A Neural Substrate of Prediction and Reward. *Science* **275**, 1593–1599 (1997).

21. Pan, P.-Y. & Ryan, T. A. Calbindin controls release probability in ventral tegmental area dopamine neurons. *Nat Neurosci* **15**, 813–815 (2012).

22. Silm, K. *et al.* Synaptic Vesicle Recycling Pathway Determines Neurotransmitter Content and Release Properties. *Neuron* **102**, 786-800.e5 (2019).

23. Pereira, D. B. *et al.* Fluorescent false neurotransmitter reveals functionally silent dopamine vesicle clusters in the striatum. *Nat Neurosci* **19**, 578–586 (2016).

24. Liu, C., Kershberg, L., Wang, J., Schneeberger, S. & Kaeser, P. S. Dopamine Secretion Is Mediated by Sparse Active Zone-like Release Sites. *Cell* **172**, 706-718.e15 (2018).

25. Banerjee, A. *et al.* Molecular and functional architecture of striatal dopamine release sites. *Neuron* 2020.11.25.398255 (2022) doi:10.1016/j.neuron.2021.10.028.

26. Kershberg, L., Banerjee, A. & Kaeser, P. S. Protein composition of axonal dopamine release sites in the striatum. *eLife* **11**, e83018 (2022).

27. Jain, S. *et al.* Adaptor protein-3 produces synaptic vesicles that release phasic dopamine. *Proc. Natl. Acad. Sci. United States Am.* **120**, e2309843120 (2023).

28. Voglmaier, S. M. *et al.* Distinct Endocytic Pathways Control the Rate and Extent of Synaptic Vesicle Protein Recycling. *Neuron* **51**, 71–84 (2006).

29. Kim, S. H. & Ryan, T. A. Synaptic vesicle recycling at CNS snapses without AP-2. *J. Neurosci. : Off. J. Soc. Neurosci.* **29**, 3865–74 (2009).

30. Xu, H. *et al.* Adaptor protein AP-3 produces synaptic vesicles that release at high frequency by recruiting phospholipid flippase ATP8A1. *Nat. Neurosci.* 1–16 (2023) doi:10.1038/s41593-023-01434-0.

31. Lavoie, N. *et al.* Vesicular Zinc Regulates the Ca 2+ Sensitivity of a Subpopulation of Presynaptic Vesicles at Hippocampal Mossy Fiber Terminals. *J. Neurosci.* **31**, 18251–18265 (2011).

32. Hnasko, T. S. *et al.* Vesicular Glutamate Transport Promotes Dopamine Storage and Glutamate Corelease In Vivo. *Neuron* **65**, 643–656 (2010).

33. Stuber, G. D., Hnasko, T. S., Britt, J. P., Edwards, R. H. & Bonci, A. Dopaminergic Terminals in the Nucleus Accumbens But Not the Dorsal Striatum Corelease Glutamate. *J Neurosci* **30**, 8229–8233 (2010).

34. Chuhma, N., Mingote, S., Moore, H. & Rayport, S. Dopamine Neurons Control Striatal Cholinergic Neurons via Regionally Heterogeneous Dopamine and Glutamate Signaling. *Neuron* **81**, 901–912 (2014).

35. Gan, Q. & Watanabe, S. Synaptic Vesicle Endocytosis in Different Model Systems. *Front Cell Neurosci* **12**, 171 (2018).

36. Weston, M. C., Nehring, R. B., Wojcik, S. M. & Rosenmund, C. Interplay between VGLUT Isoforms and Endophilin A1 Regulates Neurotransmitter Release and Short-Term Plasticity. *Neuron* **69**, 1147–1159 (2011).

37. Jr., R. T. F. *et al.* Vesicular Glutamate Transporters 1 and 2 Target to Functionally Distinct Synaptic Release Sites. *Science* **304**, 1815–1819 (2004).

38. Gronborg, M. *et al.* Quantitative Comparison of Glutamatergic and GABAergic Synaptic Vesicles Unveils Selectivity for Few Proteins Including MAL2, a Novel Synaptic Vesicle Protein. *J Neurosci* **30**, 2–12 (2010).

39. Yang, H., Wang, H. & Jaenisch, R. Generating genetically modified mice using CRISPR/Cas-mediated genome engineering. *Nat. Protoc.* **9**, 1956–1968 (2014).

40. Huttner, W. B., Schiebler, W., Greengard, P. & Camilli, P. D. Synapsin I (protein I), a nerve terminal-specific phosphoprotein. III. Its association with synaptic vesicles studied in a highly purified synaptic vesicle preparation. *J Cell Biology* **96**, 1374–1388 (1983).

41. Zhang, S. *et al.* Dopaminergic and glutamatergic microdomains in a subset of rodent mesoaccumbens axons. *Nat Neurosci* **18**, 386–392 (2015).

42. Lapios, P. *et al.* Cryo-correlative light and electron tomography of dopaminergic axonal varicosities reveals non-synaptic modulation of cortico-striatal synapses. *bioRxiv* 2025.02.07.637058 (2025) doi:10.1101/2025.02.07.637058.

43. Larhammar, M. *et al.* SLC10A4 Is a Vesicular Amine-Associated Transporter Modulating Dopamine Homeostasis. *Biol Psychiat* **77**, 526–536 (2015).

44. Amilhon, B. *et al.* VGLUT3 (Vesicular Glutamate Transporter Type 3) Contribution to the Regulation of Serotonergic Transmission and Anxiety. *J Neurosci* **30**, 2198–2210 (2010).

45. Kaeser-Woo, Y. J. *et al.* Synaptotagmin-12 Phosphorylation by cAMP-Dependent Protein Kinase Is Essential for Hippocampal Mossy Fiber LTP. *J Neurosci* **33**, 9769–9780 (2013).

46. Maximov, A., Shin, O.-H., Liu, X. & Südhof, T. C. Synaptotagmin-12, a synaptic vesicle phosphoprotein that modulates spontaneous neurotransmitter release. *J Cell Biology* **176**, 113–124 (2007).

47. Xu, J., Mashimo, T. & Südhof, T. C. Synaptotagmin-1, -2, and -9: Ca2+ Sensors for Fast Release that Specify Distinct Presynaptic Properties in Subsets of Neurons. *Neuron* **54**, 567–581 (2007).

48. Meijer, M. *et al.* Tomosyns attenuate SNARE assembly and synaptic depression by binding to VAMP2-containing template complexes. *Nat. Commun.* **15**, 2652 (2024).

49. Sauvola, C. W., Akbergenova, Y., Cunningham, K. L., Aponte-Santiago, N. A. & Littleton, J. T. The decoy SNARE Tomosyn sets tonic versus phasic release properties and is required for homeostatic synaptic plasticity. *eLife* **10**, e72841 (2021).

50. Arkan, S., Ljungberg, M., Kirik, D. & Hansen, C. DNAJB6 suppresses alpha-synuclein induced pathology in an animal model of Parkinson's disease. *Neurobiol. Dis.* **158**, 105477 (2021).

51. Aprile, F. A. *et al.* The molecular chaperones DNAJB6 and Hsp70 cooperate to suppress α-synuclein aggregation. *Sci Rep-uk* **7**, 9039 (2017).

52. Ng, J. *et al.* DNAJC6 Mutations Disrupt Dopamine Homeostasis in Juvenile Parkinsonism-Dystonia. *Mov. Disord.* **35**, 1357–1368 (2020).

53. Fjorback, A. W., Müller, H. K., Haase, J., Raarup, M. K. & Wiborg, O. Modulation of the dopamine transporter by interaction with Secretory Carrier Membrane Protein 2. *Biochem. Biophys. Res. Commun.* **406**, 165–170 (2011).

54. Cheramy, A., Leviel, V. & Glowinski, J. Dendritic release of dopamine in the substantia nigra. *Nature* **289**, 537–543 (1981).

55. Nirenberg, M. J., Chan, J., Liu, Y., Edwards, R. H. & Pickel, V. M. Ultrastructural Localization of the Vesicular Monoamine Transporter-2 in Midbrain Dopaminergic Neurons: Potential Sites for Somatodendritic Storage and Release of Dopamine. *J. Neurosci.* **16**, 4135–4145 (1996).

56. Burger, S. *et al.* Co-expression studies of the orphan carrier protein Slc10a4 and the vesicular carriers VAChT and VMAT2 in the rat central and peripheral nervous system. *Neuroscience* **193**, 109–121 (2011).

57. Fremeau, R. T. *et al.* The Expression of Vesicular Glutamate Transporters Defines Two Classes of Excitatory Synapse. *Neuron* **31**, 247–260 (2001).

58. Land, P. W., Kyonka, E. & Shamalla-Hannah, L. Vesicular glutamate transporters in the lateral geniculate nucleus: expression of VGLUT2 by retinal terminals. *Brain Res.* **996**, 251–254 (2004).

59. Graziano, A., Liu, X., Murray, K. D. & Jones, E. G. Vesicular glutamate transporters define two sets of glutamatergic afferents to the somatosensory thalamus and two thalamocortical projections in the mouse. *J Comp Neurol* **507**, 1258–1276 (2008).

60. Delattre, S. Igniting New Confocal Imaging Potential – Nikon AX R Series with NSPARC. *Microsc. Today* **31**, 23–27 (2023).

61. Zhao, H. *et al.* SCAMP5 Plays a Critical Role in Synaptic Vesicle Endocytosis during High Neuronal Activity. *J Neurosci* **34**, 10085–10095 (2014).

62. Park, D. *et al.* Impairment of Release Site Clearance within the Active Zone by Reduced SCAMP5 Expression Causes Short-Term Depression of Synaptic Release. *Cell Reports* **22**, 3339–3350 (2018).

63. Miesenböck, G., Angelis, D. A. D. & Rothman, J. E. Visualizing secretion and synaptic transmission with pH-sensitive green fluorescent proteins. *Nature* **394**, 192–195 (1998).

64. Paget-Blanc, V. *et al.* A synaptomic analysis reveals dopamine hub synapses in the mouse striatum. *Nat Commun* **13**, 3102 (2022).

65. Hobson, B. D. *et al.* Subcellular proteomics of dopamine neurons in the mouse brain. *Elife* **11**, e70921 (2022).

66. Biesemann, C. *et al.* Proteomic screening of glutamatergic mouse brain synaptosomes isolated by fluorescence activated sorting. *EMBO J.* **33**, 157–170 (2014).

67. Sugita, S. *et al.* Synaptotagmin VII as a Plasma Membrane Ca2+ Sensor in Exocytosis. *Neuron* **30**, 459–473 (2001).

68. Ruhl, D. A. *et al.* Synaptotagmin 17 controls neurite outgrowth and synaptic physiology via distinct cellular pathways. *Nat Commun* **10**, 3532 (2019).

69. Dean, C. *et al.* Axonal and dendritic synaptotagmin isoforms revealed by a pHluorin-syt functional screen. *Mol. Biol. Cell* **23**, 1715–1727 (2012).

70. Wu, Y.-J. *et al.* Syntaxin 1B is important for mouse postnatal survival and proper synaptic function at the mouse neuromuscular junctions. *J. Neurophysiol.* **114**, 2404–2417 (2015).

71. Fernández-Chacón, R. *et al.* The Synaptic Vesicle Protein CSPα Prevents Presynaptic Degeneration. *Neuron* **42**, 237–251 (2004).

72. Lopez-Ortega, E., Ruiz, R. & Tabares, L. CSPα, a Molecular Co-chaperone Essential for Short and Long-Term Synaptic Maintenance. *Front Neurosci-switz* **11**, 39 (2017).

73. Crowder, K. M. *et al.* Abnormal neurotransmission in mice lacking synaptic vesicle protein 2A (SV2A). *Proc. Natl. Acad. Sci.* **96**, 15268–15273 (1999).

74. Chandra, S., Gallardo, G., Fernández-Chacón, R., Schlüter, O. M. & Südhof, T. C. α-Synuclein Cooperates with CSPα in Preventing Neurodegeneration. *Cell* **123**, 383–396 (2005).

75. Caló, L. *et al.* CSPα reduces aggregates and rescues striatal dopamine release in αsynuclein transgenic mice. *Brain* **144**, awab076- (2021).

76. Chen, C., Arai, I., Satterfield, R., Young, S. M. & Jonas, P. Synaptotagmin 2 Is the Fast Ca2+ Sensor at a Central Inhibitory Synapse. *Cell Reports* **18**, 723–736 (2017).

77. Bouhours, B., Gjoni, E., Kochubey, O. & Schneggenburger, R. Synaptotagmin2 (Syt2) Drives Fast Release Redundantly with Syt1 at the Output Synapses of Parvalbumin-Expressing Inhibitory Neurons. *J Neurosci* **37**, 4604–4617 (2017).

78. Pennuto, M., Bonanomi, D., Benfenati, F. & Valtorta, F. Synaptophysin I Controls the Targeting of VAMP2/Synaptobrevin II to Synaptic Vesicles. *Mol. Biol. Cell* **14**, 4909–4919 (2003).

79. Wang, C. *et al.* Structure and topography of the synaptic V-ATPase–synaptophysin complex. *Nature* **631**, 899–904 (2024).

80. Harper, C. B., Blumrich, E.-M. & Cousin, M. A. Synaptophysin controls synaptobrevin-II retrieval via a cryptic C-terminal interaction site. *J. Biol. Chem.* **296**, 100266 (2021).

81. Janz, R. *et al.* Essential Roles in Synaptic Plasticity for Synaptogyrin I and Synaptophysin I. *Neuron* **24**, 687–700 (1999).

82. Raja, M. K. *et al.* Elevated synaptic vesicle release probability in synaptophysin/gyrin family quadruple knockouts. *Elife* **8**, e40744 (2019).

83. Lee, U. *et al.* SCAMP5 plays a critical role in axonal trafficking and synaptic localization of NHE6 to adjust quantal size at glutamatergic synapses. *Proc National Acad Sci* **118**, e2011371118 (2021).

84. Liao, H. *et al.* Nonredundant function of secretory carrier membrane protein isoforms in dense core vesicle exocytosis. *Am. J. Physiol.-Cell Physiol.* **294**, C797–C809 (2008).

85. Müller, H. K., Wiborg, O. & Haase, J. Subcellular Redistribution of the Serotonin Transporter by Secretory Carrier Membrane Protein 2*. *J. Biol. Chem.* **281**, 28901–28909 (2006).

86. Fujise, K., Mishra, J., Rosenfeld, M. S. & Rafiq, N. M. Synaptic vesicle characterization of iPSC-derived dopaminergic neurons provides insight into distinct secretory vesicle pools. *npj Park.'s Dis.* **11**, 16 (2025).

87. Fortin, G. M. *et al.* Segregation of dopamine and glutamate release sites in dopamine neuron axons: regulation by striatal target cells. *FASEB J.* **33**, 400–417 (2019).

88. Bo, G. D. *et al.* Dopamine neurons in culture express VGLUT2 explaining their capacity to release glutamate at synapses in addition to dopamine. *J. Neurochem.* **88**, 1398–1405 (2004).

89. Bérubé-Carrière, N. *et al.* The dual dopamine-glutamate phenotype of growing mesencephalic neurons regresses in mature rat brain. *J. Comp. Neurol.* **517**, 873–891 (2009).

90. Forlano, P. M. & Woolley, C. S. Quantitative analysis of pre- and postsynaptic sex differences in the nucleus accumbens. *J. Comp. Neurol.* **518**, 1330–1348 (2010).

91. Mingote, S., Amsellem, A., Kempf, A., Rayport, S. & Chuhma, N. Dopamine-glutamate neuron projections to the nucleus accumbens medial shell and behavioral switching. *Neurochem Int* **129**, 104482 (2019).

92. Warlow, S. M. *et al.* Mesoaccumbal glutamate neurons drive reward via glutamate release but aversion via dopamine co-release. *Neuron* **112**, 488-499.e5 (2024).

93. Poulin, J.-F. *et al.* Mapping projections of molecularly defined dopamine neuron subtypes using intersectional genetic approaches. *Nat Neurosci* **21**, 1260–1271 (2018).

94. Mendez, J. A. *et al.* Developmental and target-dependent regulation of vesicular glutamate transporter expression by dopamine neurons. *J Neurosci Official J Soc Neurosci* **28**, 6309–18 (2008).

95. Ducrot, C. *et al.* Dopaminergic neurons establish a distinctive axonal arbor with a majority of non-synaptic terminals. *Faseb J* **35**, e21791 (2021).

96. Scheuber, A. *et al.* Loss of AP-3 function affects spontaneous and evoked release at hippocampal mossy fiber synapses. *Proc. Natl. Acad. Sci.* **103**, 16562–16567 (2006).

97. Newell-Litwa, K. *et al.* Hermansky-Pudlak Protein Complexes, AP-3 and BLOC-1, Differentially Regulate Presynaptic Composition in the Striatum and Hippocampus. *J. Neurosci.* **30**, 820–831 (2010).

98. Hua, Z. *et al.* v-SNARE Composition Distinguishes Synaptic Vesicle Pools. *Neuron* **71**, 474–487 (2011).

99. Binotti, B. *et al.* ATG9 resides on a unique population of small vesicles in presynaptic nerve terminals. *Autophagy* (2023) doi:10.1080/15548627.2023.2274204.

100. Newell-Litwa, K., Salazar, G., Smith, Y. & Faundez, V. Roles of BLOC-1 and Adaptor Protein-3 Complexes in Cargo Sorting to Synaptic Vesicles. *Mol. Biol. Cell* **20**, 1441–1453 (2009).

101. Alvarez-Castelao, B. *et al.* Cell-type-specific metabolic labeling of nascent proteomes in vivo. *Nat Biotechnol* **35**, 1196–1201 (2017).

102. Moffat, J. *et al.* A Lentiviral RNAi Library for Human and Mouse Genes Applied to an Arrayed Viral High-Content Screen. *Cell* **124**, 1283–1298 (2006).

103. Guan, S., Price, J. C., Prusiner, S. B., Ghaemmaghami, S. & Burlingame, A. L. A Data Processing Pipeline for Mammalian Proteome Dynamics Studies Using Stable Isotope Metabolic Labeling*. *Mol. Cell. Proteom.* **10**, M111.010728 (2011).

104. Clauser, K. R., Baker, P. & Burlingame, A. L. Role of Accurate Mass Measurement (±10 ppm) in Protein Identification Strategies Employing MS or MS/MS and Database Searching. *Anal. Chem.* **71**, 2871–2882 (1999).